Results of Ring Compression Tests

Spent Fuel and Waste Disposition

Prepared for
US Department of Energy
Spent Fuel and Waste Science and Technology

Argonne National Laboratory
M.C. Billone and T.A. Burtseva

September 28, 2018
SFWD-SFWST-2018-000510
ANL-18/36

SUMMARY

Previous results for ZIRLO™ (now ZIRLO®) cladding from high-burnup (HBU) fuel rods suggest that the ductility transition temperature (DTT) is highly sensitive to the peak cladding hoop stress in the range of 90±3 MPa following slow cooling under decreasing stress from peak cladding temperatures (PCTs) of 400°C and 350°C. In particular, the DTT was <30°C for peak cladding hoop stresses of 88±1 MPa and ≥125°C for peak cladding hoop stresses of 93 MPa and 94 MPa. However, the hydrogen content was lower (390–530 wppm) for the lower stresses and higher (560–650 wppm) for the higher stresses. In order to confirm this narrow stress dependence, two additional tests are planned: (a) 350-wppm ZIRLO™ subjected to peak conditions of 350°C/93-MPa and (b) 650-wppm ZIRLO™ subjected to peak conditions of 350°C/87-MPa. These tests could not be conducted during FY2018 because of equipment problems. They will be conducted during FY2019 after equipment repair and/or replacement.

The current experimental work consists of: (a) ring compression tests (RCTs) with as-fabricated M5® cladding to determine the unloading slope for a range of sample dimensions, displacement rates, test temperatures, and maximum displacements; (b) RCTs with HBU-fuel ZIRLO™ samples to determine the reduction of the unloading slope due to minor cracking (e.g., multiple cracks that are 10–20% of the cladding wall thickness); and (c) determination of the ductility of HBU-fuel ZIRLO™ cladding with hydrogen contents of 350 wppm and 650 wppm.

The offset displacement, which is used as a measure of ductility after normalization to the cladding metal outer diameter, is the net displacement along the zero load axis between the loading slope and the unloading slope. The traditional approach is to assume that the unloading slope is equal to the loading slope. This approach has been validated experimentally and by finite element analysis (FEA) for axial-tension and axial-bend tests. However, for the RCT, the unloading slope is always less than the loading slope for displacements in the elastic-plastic regime. It decreases with increased plastic displacement and it decreases with minor cracking prior to major cracking. In order to quantify the decrease in loading slope with plastic displacement, thirty tests were conducted with 17×17 and 15×15 M5® cladding with a range of dimensional parameters (outer diameter, wall thickness, and length) and test conditions (displacement rate, maximum displacement, and temperature). The results showed a consistent reduction in measured unloading slope relative to the measured loading slope of up to 25% at traditional offset strains of 8%, beyond which the ratio was essentially constant. These results are consistent results obtained using HBU-fuel M5® samples that did not crack. They are relevant and useful not only for the current experimental work with irradiated 17×17 cladding alloys, but they are also needed for writing the ASTM guidance document on RCTs.

HBU-fuel ZIRLO™ cladding segment 105G was characterized and tested in the as-irradiated condition. The outer diameter, oxide layer thickness (≈60 μm), and metal wall thickness were essentially the same as for the adjacent 105F segment, which had about 650 wppm hydrogen and was characterized and tested in FY2015. Hydrides were predominately oriented in the circumferential direction with isolated, sparsely distributed, short (<10% of the cladding wall) radial hydrides. Such radial hydrides have been observed in M5® and ZIRLO™ cladding from fuel rods irradiated to HBU. Rings tested at 5 mm/s and at 90°C and 120°C exhibited full ductility of about 10% through 1.7-mm displacement. The sample tested at 90°C showed a gradual load drop of 15% following the peak load, which is due to minor cracking through the hydride rim and along circumferential hydrides. Use of the corrected unloading slope developed for compressed cladding without cracks resulted in an over-prediction of 2.5% strain relative to the permanent strain based on the directly measured post-test change in diameter. For the sample tested at 120°C, the gradual load drop was only 7%, indicating fewer and shorter cracks. The ductility over-

prediction was about the same (2.8%) for this ring. An algorithm was developed to bring the offset strain to within 0.4% of the measured permanent strain. It was tested using the load-displacement data for the 25°C test, which exhibited a 25% total load drop in three stages. To assist in data interpretation, an additional 25°C test was conducted at 0.05 mm/s, which allowed termination of the test following a 26% load drop. Use of the algorithm resulted in an offset strain that was within 0.5% of the directly measured permanent strain. The algorithm will be tested against a large number of load-displacement curves exhibiting a gradual load drop throughout the 1.7-mm displacement and those exhibiting a gradual load drop prior to a very steep load drop.

The 650-wppm ZIRLO™ (105G) samples compressed at 25°C were surprisingly ductile (7% offset and permanent strains). These results suggest that radial hydrides were the primary cause of the low ductility exhibited by 105F samples following 350°C and 94-MPa heat treatment. The results were comparable to those presented previously for the 350-wppm ZIRLO™ (646C) samples, which had been subjected to a 24-hour anneal at 350°C and cooling at a hoop stress (<70 MPa) too low to induce radial hydride precipitation. Given that these cladding samples were from 4-cycle fuel rods with a very high linear heat rating during the 4^{th} cycle, the hydride rim was very dense with a small fraction of hydrides below the rim. Fuel rods operated at lower linear heat rating have a less concentrated hydride distribution. It has been shown that a higher concentration of circumferential hydrides across the cladding wall results in more extensive cracking at lower plastic strains. Results from sister-rod testing will include a range of lower- and higher-power fuel rods and they will provide the opportunity to determine the effects of the circumferential hydride distribution on cladding ductility.

CONTENTS

FIGURES

TABLES

ACRONYMS, UNITS AND SYMBOLS

ACRONYMS

AF	as-fabricated
ANL	Argonne National Laboratory
CWSRA	cold-worked, stress-relief annealed
DBTT	ductile-to-brittle transition temperature
DOE	U.S. Department of Energy
DTT	ductility transition temperature
EOL	end of life
EPRI	Electric Power Research Institute
FEA	finite element analysis
HBU	high burnup
IFBA	Integral Fuel Burnable Absorber
ISG	Interim Staff Guidance
NRC	Nuclear Regulatory Commission
PCMI	pellet-cladding mechanical interaction
PCT	peak cladding temperature
PIE	post-irradiation examinations
PNNL	Pacific Northwest National Laboratory
PWR	pressurized water reactor
RCT	ring compression test
RHCF	radial hydride continuity factor (%)
RHT	radial-hydride treatment
RIP	rod internal pressure (MPa)
RT	room temperature
RXA	recrystallized-annealed
SFWST	Spent Fuel Waste and Science Technology
SNL	Sandia National Laboratories
TMT	thermal-mechanical treatment
Zry-2	Zircaloy-2
Zry-4	Zircaloy-4

UNITS

°C	degree Celsius
GWd/MTU	giga-watt-days per metric tonne of uranium
h	hour
K	degree Kelvin
kN	kilo-newton
m	meter
mm	millimeter
µm	micro meter (micron)
MPa	mega-pascal
N	newton
s	second
wppm	weight parts per million

SYMBOLS

C_H	total hydrogen content in weight parts per million (wppm)
C_{HD}	dissolved hydrogen content at temperature T_D during heating (wppm)
C_{HP}	dissolved hydrogen content (wppm) needed to initiate hydride precipitation during cooling at temperature T_P
D_{mi}	inner diameter of cladding alloy (mm)
D_{mo}	outer diameter of cladding alloy (mm)
D_o	cladding outer diameter (includes outer-surface oxide layer if present, mm)
d_p	permanent displacement (pre-test minus post-test diameter in loading direction, mm)
d_p/D_{mo}	permanent strain (%)
δ	controlled sample displacement (mm) at the 12 o'clock sample position
δ_e	elastic displacement (mm)
δ_{max}	maximum sample displacement (mm) at the 12 o'clock sample position
Δp	pressure difference across cladding wall ($p_i - p_o$, MPa)
δ_p	traditional offset displacement (mm)
δ_{pc}	corrected offset displacement (mm)
δ_p/D_{mo}	traditional offset strain (%)
δ_{pc}/D_{mo}	corrected offset strain (%)
ΔT	temperature drop per drying cycle (°C)
ΔT_{PD}	difference between hydride precipitation (T_P) and dissolution (T_D) temperatures (°C)
E	Young's modulus (GPa)
$(\varepsilon_\theta)_{max}$	maximum hoop strain
h_m	cladding alloy wall thickness (mm)
h_{ox}	thickness of outer surface oxide layer (μm)
K_{LC}	calculated loading slope (i.e., loading stiffness) for RCT samples (kN/mm)
K_{LM}	measured linearized loading slope (kN/mm)
K_U	calculated linearized unloading slope (kN/mm)
K_{UM}	measured linearized unloading slope (kN/mm)
L	length of RCT sample (mm)
M_{max}	maximum RCT bending moment (N•m)
v	Poisson's ratio
P	measured RCT load at the 12 o'clock sample position (N)
P_1	load prior to steep load drop
P_e	load during elastic displacement (N)
p_i	internal gas pressure (MPa)
P_{max}	maximum RCT load (N)
p_o	external gas pressure
R_{mi}	inner radius of cladding alloy (mm)
R_{mid}	mid-wall radius of cladding alloy (mm)
σ_θ	hoop stress (MPa)
T	temperature (°C)
T_D	hydrogen dissolution temperature (°C)
T_P	hydrogen precipitation temperature (°C)

Page intentionally blank

1. INTRODUCTION

Structural analyses of high-burnup (HBU) fuel rods require cladding mechanical properties and failure limits to assess fuel behavior during long-term dry-cask storage, post-storage retrieval and transportation, and post-transport retrieval. License applications for transport casks containing HBU fuel assemblies with Zircaloy-2 (Zry-2), Zircaloy-4 (Zry-4) and ZIRLO® cladding have used properties and failure limits for as-irradiated cladding [1,2]. Reliable mechanical properties are not currently available for as-fabricated or irradiated M5® cladding. These properties will be determined for irradiated M5® cladding in the sister-rod test program. Pre-storage drying-transfer operations and early stage storage subject cladding to higher tensile hoop stresses induced by higher temperatures and pressures relative to in-reactor operation and pool storage. Under these conditions, radial hydrides may precipitate during slow cooling and may introduce an embrittlement mechanism if the cladding temperature decreases below a critical point, which is defined in this work as the ductility transition temperature (DTT) and which was referred to as the ductile-to-brittle transition temperature (DBTT) in previous reports. DTT was introduced to avoid potential confusion among materials experts who associate DBTT with body-centered-cubic metals. If embrittlement is predicted to occur, then failure hoop stresses and strains would have to be revised to account for this effect.

In Interim Staff Guidance-11, Revision 3 (ISG-11, Rev. 3), the Nuclear Regulatory Commission (NRC) recommends a peak cladding temperature (PCT) limit of 400°C for high-burnup (≥45 GWd/MTU) fuel under normal conditions of storage and short-term loading operations (e.g., drying, backfilling with inert gas, and transferring the canister or cask to the storage pad) [3]. During loading operations, repeated thermal cycling (repeated heat-up/cool-down cycles) may occur but should be limited to fewer than 10 cycles, with cladding temperature variations (ΔT) that are less than 65°C per cycle, according to ISG-11, Rev. 3 (see Fig. 1 for justification of ΔT <65°C per cycle). One concern for high-burnup (HBU) fuel cladding is the possible precipitation of radial hydrides, which could embrittle cladding in response to tensile hoop stresses caused by internal pressure loading and "pinch-type" loading during transport. Limits established in ISG-11, Rev. 3, relied on data available before 2002, which were primarily for low-burnup and non-irradiated/pre-hydrided Zry-4. NUREG-2224 [4], which was recently released for public comment, is more up to date and more extensive in terms of supporting data and analyses. It maintains the recommendation of 400°C PCT for high-burnup (HBU) fuel.

Argonne National Laboratory (ANL) has developed a test protocol for studying HBU-fuel cladding embrittlement that has been used to generate data for NRC. Experimentally, the protocol involves two steps: (a) radial-hydride treatment (RHT), during which HBU-fuel cladding is exposed to simulated drying-storage temperature and hoop stress conditions, including slow cooling with decreasing stress, followed by (b) ring compression testing, in which rings sectioned from RHT HBU-fuel cladding are compressed to determine strength and ductility as a function of test temperature. The ring compression test (RCT) is used primarily as a ductility screening test, and the RCT loading simulates the pinch-type loading on HBU-fuel cladding that occurs during normal conditions of cask transport and potential drop accidents. The protocol was used to generate DTT data for HBU-fuel ZIRLO™ and Zry-4 [5, 6] (both efforts sponsored by NRC) and HBU-fuel M5® (sponsored by the U.S. Department of Energy [DOE]) [7]. Under DOE-sponsorship, ANL has also generated baseline characterization data and data for the strength and ductility of as-irradiated HBU-fuel Zry-4, ZIRLO™, and M5®. These data are important not only for determining the potentially degrading effects of drying and early stage storage, but also for serving as reference properties for future evaluations of the effects of drying storage on these cladding alloys [8–10]. Reference 11 documents ANL data generated through September 30, 2013, including additional DOE-sponsored test results for HBU-fuel ZIRLO™ and M5® following cooling from 400°C and lower hoop stress levels (80 to 90 MPa). Reference 12 contains refined interpretations of previously

generated data, as well as test results for HBU-fuel ZIRLO™ subjected to 3-cycle drying at 350°C PCT and 93-MPa peak hoop stress. Reference 13 contains additional data for as-irradiated HBU-fuel Zry-4 and for HBU-fuel ZIRLO™ following 1-cycle drying at 350°C PCT and 94-MPa peak hoop stress. Reference 14 presents results generated for HBU-fuel ZIRLO™ and M5® following RHT at 350°C and peak stresses in the range of 87-89 MPa. In Reference 15, the issue of continuity of radial hydrides in the axial direction is addressed.

ANL test results indicate that susceptibility to radial-hydride precipitation during cooling is dependent on cladding alloy, thermal-mechanical treatment (TMT), total hydrogen content (C_H), C_H below the hydride rim, and peak RHT temperature and hoop stress. The combination of recrystallized-annealed (RXA) microstructure and low C_H results in higher susceptibility of M5® to precipitation of long radial hydrides during cooling. For cold-worked, stress-relief-annealed (CWSRA) alloys, ZIRLO™ was found to be more susceptible to radial-hydride precipitation than Zry-4. The differences in the distribution of hydrides across the cladding wall (lower for ZIRLO™ below the hydride rim) may be partly responsible for this behavior [6].

Section 2 of this report describes the materials and test methods used in this program. It has been updated with RCT results for 30 new benchmark tests using as-fabricated 17×17 and 15×15 M5® samples with a range of outer diameters (9.49–10.91 mm), wall thicknesses (0.57–0.63 mm) and lengths (6–10 mm). Test variables included displacement rate (0.05 mm/s and 5 mm/s), maximum displacement (0.3–2.0 mm), and temperature (25°C and 120°C). These tests were conducted with both the Instron 5566 screw-type machine, whose calibration was recently verified, and the in-glove-box Instron 8511 servo-hydraulic machine, which has been used to test irradiated cladding rings. Benchmark test results are used to verify calibration of the Instron-8511, to generate additional data used to determine the decrease in unloading slope (K_{UM}) relative to the loading slope (K_{LM}) with increasing displacement for rings that do not crack. The tests with larger diameter, thicker wall, and longer/shorter cladding samples were conducted to provide the basis for developing the ASTM Guidance document for how to conduct such tests and how to determine ductility from load-displacement curves. Previous test results are summarized in Section 3 for HBU-fuel ZIRLO™ subjected to RHT at 400°C PCT and 350°C PCT for a range of hydrogen contents and peak hoop stresses [14]. These results suggest a high-sensitivity of the DTT of this alloy to a narrow range of peak hoop stress (90±3 MPa) for which the DTT increases from <30°C to ≥125°C.

New ductility results for as-irradiated HBU-fuel ZIRLO™ with high hydrogen content (≈650 wppm) are presented in Section 4. These RCTs were conducted to determine the baseline ductility of high-hydrogen ZIRLO™. RCT results were also used to provide guidance on ductility decrease due to circumferential hydrides and the effects of minor cracking on the unloading stiffness. The ductility vs. temperature results for 650-wppm HBU-fuel ZIRLO™ are compared to the ductility results generated previously [15] for 350-wppm HBU-fuel ZIRLO™ and updated in the current work.

To appreciate the influence of PCT (i.e., decrease from 400°C to 350°C), stress, temperature cycling, and hydrogen content on radial hydride precipitation and embrittlement, it is important to review literature results for hydrogen dissolution and hydride precipitation. Unlike most, if not all, studies of radial hydride precipitation and subsequent ductility, the ANL RHT process includes decreasing internal gas pressure and hoop stress with decreasing temperature during cooling, as would occur in fuel rods during storage. Most researchers have used an actively pressurized cladding tube for which the pressure is kept constant during cooling. As such, it is important to understand the dependence of hydrogen solubility (C_{HD}) on temperature (T_D) during the heating phase and the content of dissolved hydrogen (C_{HP}) needed to initiate precipitation at the precipitation temperature (T_P) during the cooling phase. Figure 1

summarizes the data of Kearns [16], Kammenzind et al. [17], and McMinn et al. [18] for these parameters, as well as the temperature gap (ΔT_{PD}) between precipitation and dissolution. As shown in Fig. 1, the solubility of hydrogen at 400°C is 206±5 wppm and the precipitation temperature is 335°C. The hydrogen solubility at 350°C is 126±6 wppm and the precipitation temperature is 285°C. These results are applicable to the HBU-fuel Zry-4 and ZIRLO™ samples used in the ANL test program because these samples contained ≥300 wppm for Zry-4 and ≥350 wppm for ZIRLO™. However, the HBU-fuel M5® samples tested by ANL contained lower hydrogen contents (58–94 wppm) for which total dissolution occurred during the heating ramp at temperatures in the range of 290–330°C. Corresponding temperatures at which precipitation initiated were in the low range of 225–265°C. Also, it has been shown that dissolution and precipitation temperatures for Nb-containing alloys (Zr-1Nb alloy M5® and Zr-1Sn-0.26Nb alloy N18) were essentially the same as those measured for Zry-4 [19]. These results suggest that the data in Fig. 1 also apply to ZIRLO™. More significant than differences in alloy compositions, thermal-mechanical treatment (i.e., level of cold work) and fast-neutron damage levels are the differences in T_D and T_P measured from diffusion couples [16, 17] and those measured using differential scanning calorimetry [18, 19]. In the current work, the diffusion-couple data from long-time tests at temperature are used because they appear to be more applicable to drying and storage time frames.

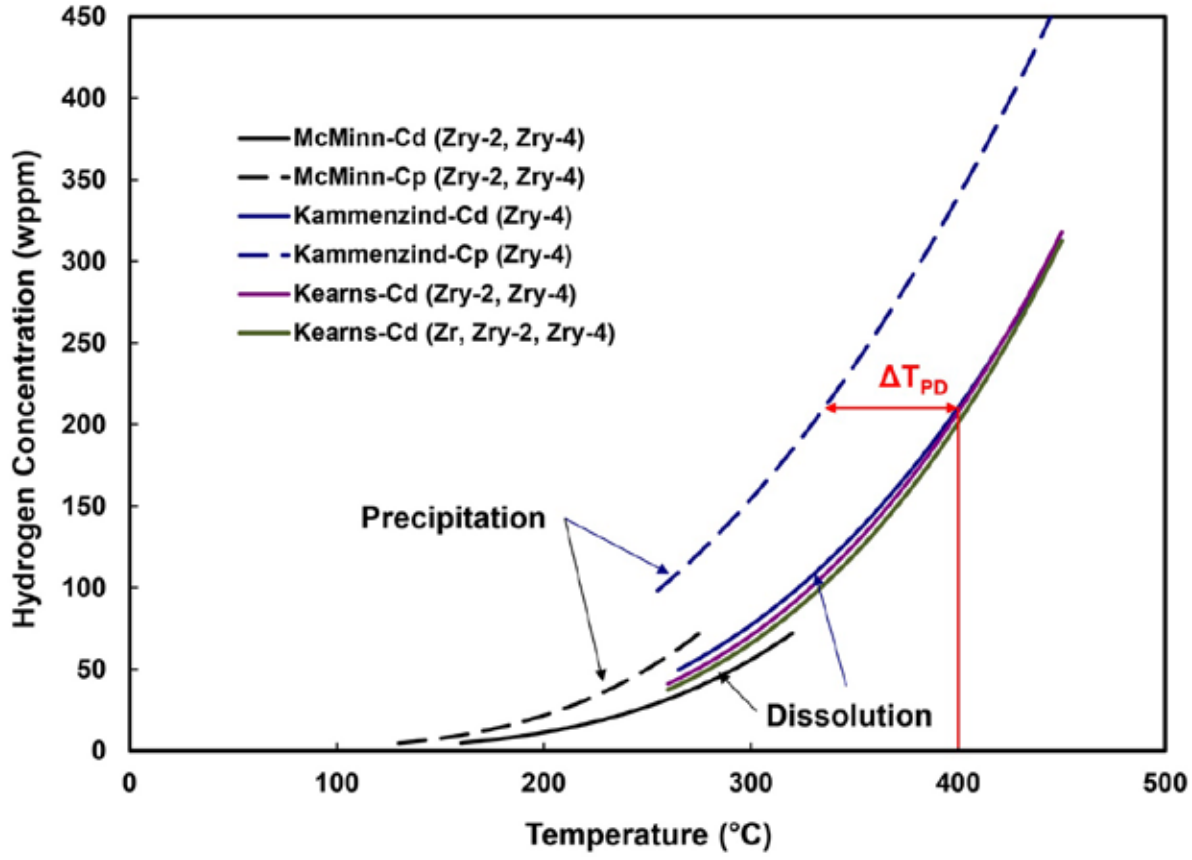

Figure 1: Steady-state curves for hydrogen dissolution and precipitation in Zr alloys.

Page intentionally blank

2. HBU-FUEL CLADDING MATERIALS AND TEST METHODS

2.1 HBU-FUEL CLADDING MATERIALS

References 11 and 12 contain detailed lists of defueled cladding materials used in previous testing. Relevant materials for the current work are listed in Table 1. The new FY2018 test material is listed in bold font. For rodlets subjected to three drying cycles, the hold time at PCT refers to the hold time per cycle. The materials came from fuel rods irradiated to HBU in commercial pressurized water reactors (PWRs). The ZIRLO™ (now ZIRLO®) cladding segments came from three fuel rods irradiated in the same assembly in the North Anna reactors. The $\pm C_H$ values represent one standard deviation in data collected from multiple axial locations along each segment and quarter-ring samples at each axial location. The large one-sigma values were due to circumferential variation in C_H, especially for average C_H values >350 wppm. Additional characterization results are presented in subsequent sections.

Table 1 Summary of HBU-fuel ZIRLO™ cladding materials used in studies of cladding ductility for as-irradiated cladding and following simulated drying and storage RHT at PCT. Axial location is the distance from the bottom of the fuel rod to the mid-span of the segment

ANL IN	Axial Location, mm	Burnup, GWd/MTU	Hydrogen Content, wppm	Peak RHT Stress, MPa	PCT, °C	Hold Time (cycles), h
646D	2628	66	387±72	87	350	24 (1)
646C	2548	66	≈350	<70	350	24 (1)
105F	3000	68	644±172	94	350	1 (1)
105G	**3080**	**68**	**≈650**	**---**	**---**	**--- (---)**

2.2 TEST METHODS

The protocol for single-cycle heating-cooling tests consisted of two steps: (a) simulated drying and storage testing RHT during which a sealed, pressurized rodlet is heated to and stabilized at the PCT within one hour, held at the PCT for 1–24 hours, cooled slowly (by laboratory standards) at 5°C/h to 200°C (≈130°C for low-C_H M5®), and cooled at a higher rate to room temperature (RT) and (b) ring-compression testing at three to four temperatures from RT to 200°C and at 5 mm/s (reference value) displacement rate to a maximum sample displacement (δ_{max}) of 1.7 mm. For three-cycle heating-cooling RHTs, rodlets were heated to the PCT, held at the PCT for one hour, cooled at 5°C/h to 100°C below the PCT, reheated to the PCT, held at PCT for one hour, cooled at 5°C/h to 100°C below the PCT, reheated to the PCT, held at the PCT for one hour, and then cooled at the same rate used for the single-cycle tests. For the last three ZIRLO™ rodlets (105F, 646D, and 646C) subjected to 350°C PCT, the 5°C/h cooling rate was maintained down to 130°C to give the dissolved hydrogen (≈125 wppm) more time to precipitate.

HBU-fuel cladding segments were used to fabricate sealed and pressurized (with argon) rodlets. Details of rodlet fabrication are given in Ref. 12. However, some details are worth repeating as fabrication problems were encountered in fabricating rodlet (646C) in FY2017. Following outer- and inner-surface oxide removal at the ends of the samples, as well as squaring of the ends, the components to be assembled are shown in Fig. 2. From left to right, these components include the solid bottom end fixture, the zirconia pellet used to reduce gas volume and stored energy, the HBU-fuel cladding segment, and the top end fixture, which has a small hole at the top to allow pressurization. In general, the fabrication sequence consists of circumferential welding of the bottom end plug, loading of the pellet, circumferential welding of the top end plug, pressurization in a chamber, laser-welding the top end-

fixture hole with the rodlet in the chamber, and checking to ensure that the rodlet is indeed sealed and holds pressure. Prior to insertion of the rodlet into the RHT furnace, the rodlet is shaken several times to give a qualitative indication that pressure was maintained. If the zirconia pellet does not move back and forth, there has to be pressure inside the rodlet. The shake test is also repeated after the RHT to ensure pressurization throughout the RHT. Previously, it had been demonstrated that an absolute pressure of 4.7 MPa was sufficient to prevent pellet movement in a HBU-fuel ZIRLO™ rodlet. To validate the shake test, four as-fabricated ZIRLO™ rodlets were made with internal pressures of 1.1 MPa to 4.0 MPa. The rodlets were shaken by the lead experimenter and the lead technician. The results were inconclusive for as-fabricated cladding with a smooth inner surface. Other factors that may affect pellet movement are the pellet outer diameter (7.9–8.2 mm) and the roughness of the cladding inner surface, which is much higher for HBU-fuel cladding. The shake test will continue to be used for HBU-fuel-cladding rodlets until a better method is developed for ensuring post-test rodlet pressurization.

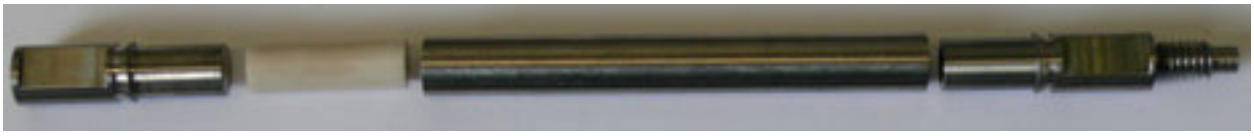

Figure 2: Rodlet components: bottom end fixture, zirconia pellet, cladding segment, and top end fixture.

Although performing the circumferential weld successfully is the most difficult rodlet fabrication step, a successful weld depends on the quality of the oxide removal, especially removal of the inner-surface oxide layer. For the long end caps shown in Fig. 2, inner-surface oxide removal must extend about 12 mm to 19 mm from each end. Inner-surface oxide removal is performed by stationary reamers with the sample rotated by a mini-lathe. With such a crude setup, it is difficult to remove all the inner-surface oxide within the span needed without thinning the cladding wall at the ends. The end caps have been redesigned such that the length of the end-cap solid cylinder that extends into the cladding has been reduced by a factor of two. There is also consideration of replacing the 10-year-old mini-lathe with a new one.

Prior to rodlet pressurization, the outer diameter is measured for each cladding segment at two orientations (90° apart) and at three axial locations. These values are averaged to give the cladding outer diameter (D_o). The thickness of the outer-surface oxide layer (h_{ox}) is estimated from sibling rod data or from interpolation or extrapolation of data from the same fuel rod at different axial locations. The same approach is used to estimate the cladding alloy wall thickness (h_m). The outer diameter of the cladding alloy (D_{mo}) is calculated from $D_o - 2\,h_{ox}$, and the cladding alloy inner diameter (D_{mi}) is calculated from $D_{mo} - 2\,h_m$. The ratio R_{mi}/h_m, where R_{mi} is the cladding alloy inner radius, is used in Eq. 1 to calculate the average hoop stress (σ_θ) from the pressure difference ($\Delta p = p_i - p_o$) across the cladding wall, where p_i and p_o (0.1 MPa during fabrication at 23°C and 0.17 MPa in the RHT furnace) are internal and external pressures, respectively.

$$\sigma_\theta = (R_{mi}/h_m)\,\Delta p - p_o \qquad (1)$$

The ideal gas law is used to relate p_i at the PCT to p_i at 23°C: $p_i(\text{PCT}) = ([\text{PCT} + 273\text{K}]/296\text{K})\; p_i(23°\text{C})$. Given the target σ_θ at the PCT, the fabrication pressure at 23°C can be calculated using Eq. 1.

Following RHT, the rodlet is depressurized and sectioned for C_H samples, RCT samples, and metallographic imaging samples, from which precise values of the geometrical parameters in Eq. 1 can be determined. Using this procedure, the calculated target peak rodlet σ_θ has been found to be within ±3 MPa of the target value.

The second phase of the test protocol consists of RCTs. Figure 3 shows a schematic of RCT loading. The RCT load induces maximum hoop bending stresses (σ_θ) at the inner surfaces of the 12 (under load) and 6 (above support) o'clock positions. Tensile hoop stresses also occur at the 3 and 9 o'clock outer surfaces. Associated with these tensile stresses are tensile strains (ε_θ). Within the elastic range, hoop stresses at 3 and 9 o'clock are about 40% less than hoop stresses at 12 and 6 o'clock. Also, because the length ($L \approx 8$ mm) of the rings is much greater than the cladding wall thickness (0.54 to 0.57 mm for HBU ZIRLO™ and M5®), an axial stress is induced that is up to 0.37 times the hoop stress within the elastic deformation regime. The maximum sample displacement ($\delta_{max} = 1.7$ mm) is chosen to give ≈10% offset strain at RT. The starting point for the RCT is 1 mm above the sample to allow the full displacement rate to develop. The reference displacement rate is 5 mm/s.

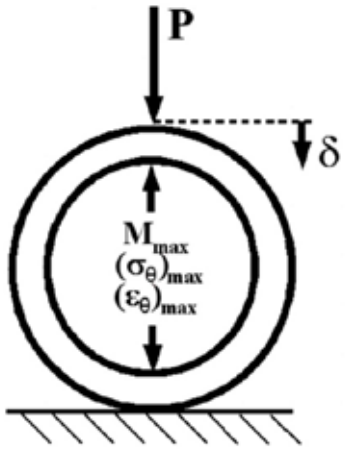

Figure 3: RCT measured load (P) and controlled displacement (δ).

Load-displacement curves and post-test diameter measurements are used to determine offset (δ_p) and permanent (d_p) displacements, respectively. These are normalized to D_{mo} to give relative plastic displacement (i.e., plastic strain) for the ring structure. Permanent displacement is defined as the difference between pre- and post-test diameter measurements along the loading direction. Figures 4 and 5 shows how traditional and corrected offset displacements are determined from benchmark load-displacement curves for as-fabricated (AF) 17×17 M5® rings subjected to displacements of 1.7-mm displacement (Fig. 4) and 0.5-mm (Fig. 5). For the benchmark samples, $D_{mo} = 9.49$ mm in the loading direction, $h_m = 0.57$ mm, and $L = 8.06$ mm. The traditional offset-displacement methodology calls for unloading the sample at the same slope as the measured linearized loading slope (K_{LM}). It should be noted that K_{LM} is less than the calculated sample stiffness (K_{LC}) due to the influence of machine compliance. For the case shown in Fig. 4, this approach gives a traditional $\delta_p = 1.24$ mm, which is greater than the more accurate $d_p = 1.10$ mm based on the difference between pre- and post-test diameters. Thus, there is an inherent error in the traditional approach as the measured linearized unloading slope (K_{UM}) is always less than K_{LM}. K_{UM} is determined from the slope of the line connecting δ_{max} to the displacement axis value based on the measured value of d_p at zero load. Normalizing these displacements to D_{mo} gives 13% traditional offset strain and 11.6% permanent strain, which is also the "corrected offset strain" (δ_{pc}) for these benchmark tests. As noted in Fig. 4, K_{UM}/K_{LM} is 0.771 for this case. As the total and traditional displacements decrease, the difference between traditional offset displacement and permanent displacement decreases. This is shown in Fig. 5 for which the uncorrected (i.e., traditional) offset displacement is 0.11 mm, the permanent displacement is 0.09 mm, and K_{UM}/K_{LM} is 0.944.

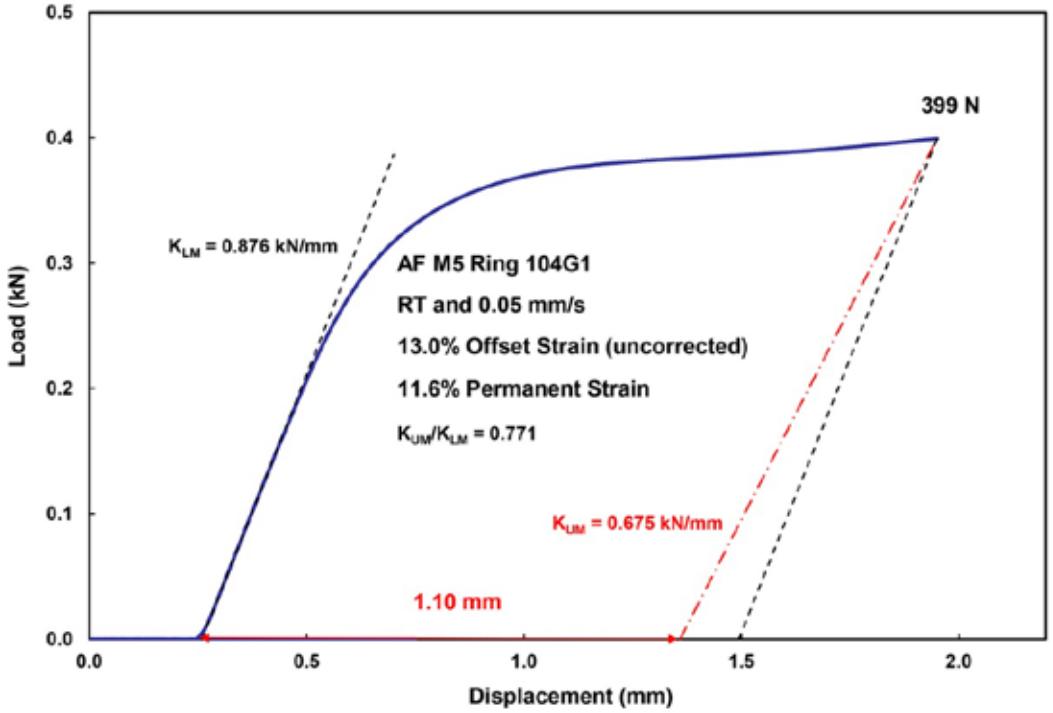

Figure 4: Load-displacement curve for as-fabricated (AF) M5® ring tested at RT and 0.05 mm/s to 1.7 mm ring displacement.

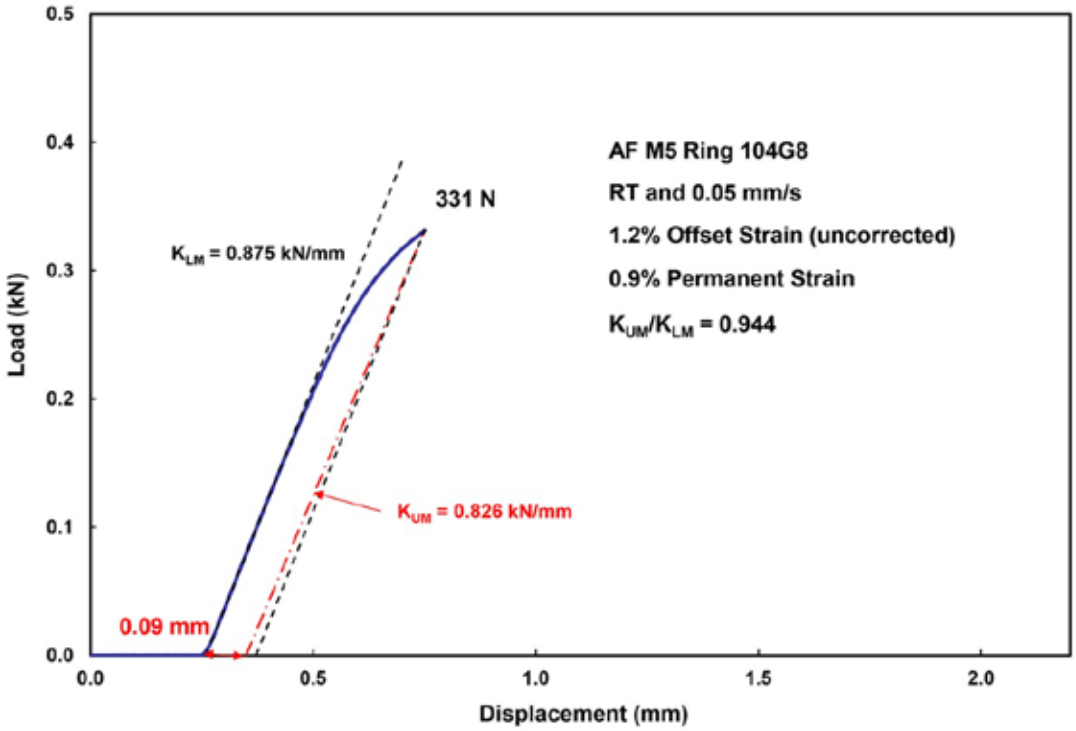

Figure 5: Load-displacement curve for AF M5® ring tested at RT and 0.05 mm/s to 0.5 mm ring displacement.

Energy methods were used to determine the bending moment as a function of circumferential orientation. Both wide-beam and narrow-beam assumptions were used to relate the bending moment to bending stresses and strains within the elastic-deformation regime, as well as the relationship between the elastic load (P_e) and elastic displacement (δ_e). The curvature of the ring was not taken into account in the bending analysis. The calculated loading stiffness is $K_{LC} = P_e/\delta_e$, where

$$P_e = \{(E\,L)/[1.79\,(1-\nu^2)]\}\,(h_m/R_{mid})^3\,\delta_e \quad (2)$$

for the wide-beam assumption and

$$P_e = \{(E\,L)/[1.79]\}\,(h_m/R_{mid})^3\,\delta_e \quad (3)$$

for the narrow-beam assumption.

In Eqs. 2 and 3, E is Young's modulus (91.9 GPa for RXA alloys [1]), ν is Poisson's ratio (0.37), and $R_{mid} = (D_{mo} - h_m)/2$ is the mid-wall radius. On the basis of finite element analysis (FEA) results for the loading stiffness, Eq. 2 over-predicts the loading stiffness by about 7% and Eq. 3 under-predicts the loading stiffness by about the same amount for $L/h_m = 13$, which is relevant to the standard length (8.0 mm) and wall thickness (0.61 mm) used for most benchmark tests. Thus, it is recommended that the average of the Eq. 2 and Eq. 3 stiffness values be used for calculating K_{LC}.

For HBU cladding rings that crack during the 1.7-mm displacement, d_p cannot be determined accurately. Thus, one must rely on a correlation for the unloading slope to determine the corrected offset displacement prior to the first significant crack, from which the ductility can be determined. The correlation developed for this application is based on the results from a large number of benchmark tests with permanent displacements ranging from 0.09 mm to 1.4 mm, displacement rates in the range of 0.03–50 mm/s, and temperatures in the range of 20–150°C. Results of these benchmark tests, including the additional tests conducted in FY2018, are shown in Fig. 6 for the ratio of measured unloading/loading (K_{UM}/K_{LM}) slopes vs. traditional offset strain (δ_p/D_{mo}). Also shown in Fig. 6 are results from nine RCTs with HBU-fuel M5® (solid red circles) that exhibited no cracking after 1.7-mm total displacement. The hollow blue-circle data points are from RCTs conducted with AF 17×17 M5® (48 points) and AF 17×17 ZIRLO™ (6 points) cladding samples. Outer diameters were 9.49±0.1 mm and nominal cladding wall thickness values were 0.61 mm (reference case) and 0.57 mm (6 ZIRLO™ data points and 15 M5® data points). The data set also includes RCT results from two machines: (a) Instron 5556 and (b) Instron 8511.

The correlation developed from an earlier limited data set for the calculated unloading slope (K_U in kN/mm) as a function of the measured loading slope (K_{LM} in kN/mm) and the measured traditional offset strain (in %) is:

$$K_U/K_{LM} = 1 - 0.02612\,\delta_p/D_{mo} \text{ for } \delta_p/D_{mo} \le 8.7\% \quad (4a)$$

$$K_U/K_{LM} = 0.773 \text{ for } \delta_p/D_{mo} > 8.7\% \quad (4b)$$

For the complete data set shown in Fig. 6 for AF samples, the stiffness ratio is 0.758 at traditional offset strains >8%. The best-fit slope at ≤8% traditional offset strain is 0.0303 as compared to 0.02612 in Eq. 4a. The stiffness ratio for HBU-fuel M5® with >8% traditional offset strain is 0.746, which is in excellent agreement with the 0.758 determined for AF cladding materials.

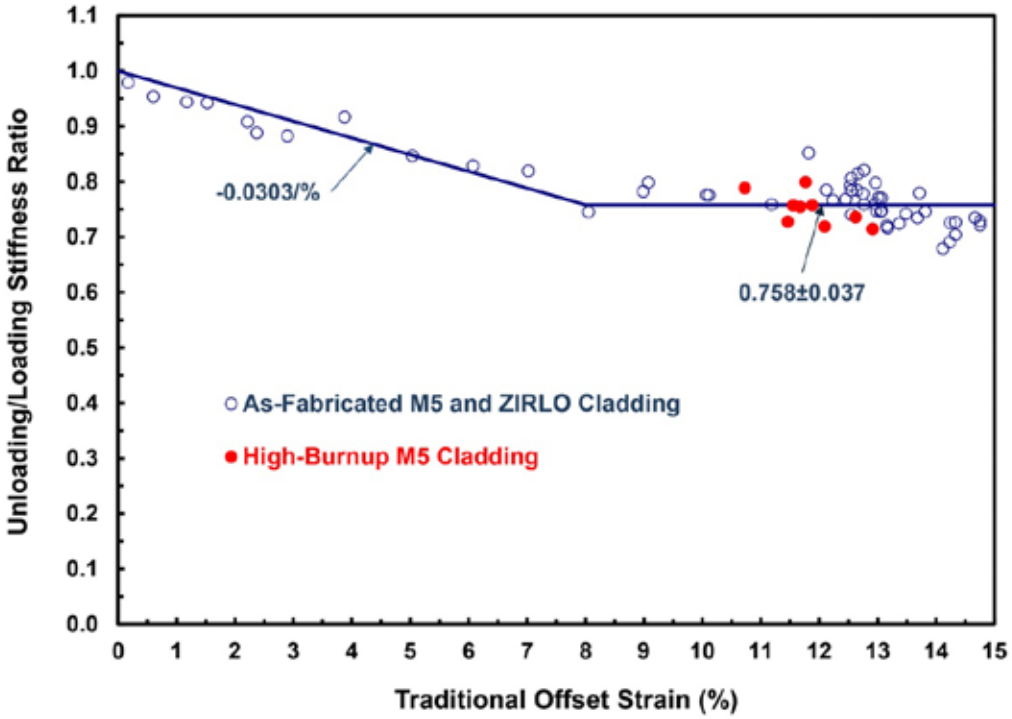

Figure 6: RCT benchmark results for determining the ratio of unloading/loading stiffness as a function of the traditional offset strain.

Additional benchmark tests were conducted with AF 17×17 M5® (0.57-mm wall) to determine the effects of sample length and with AF 15×15 M5® cladding to determine the effects of larger diameter (10.91 mm) and thicker wall (0.63 mm). Such data are important for writing the ASTM Guidance document to establish a range of parameters for which the guidance applies. As shown in Fig. 7, the results from the shorter (6-mm-long) and longer (10-mm-long) samples are consistent with the K_U/K_{LM} trend curve from Fig. 6, as are the results shown in Fig. 8 for the larger-diameter/thicker-wall cladding.

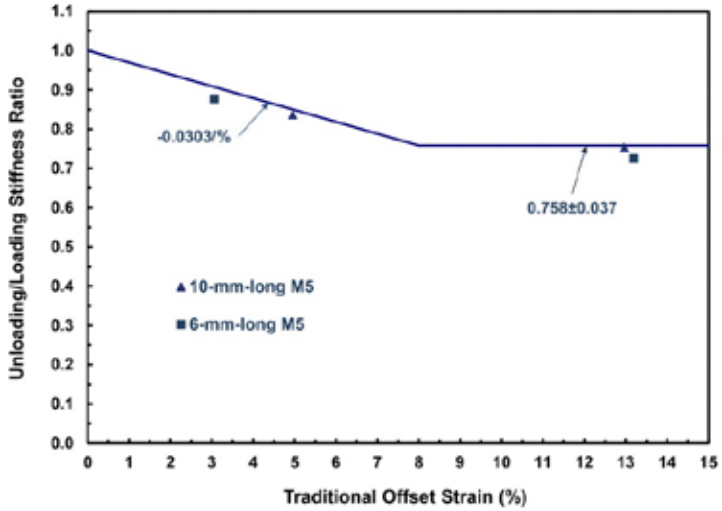

Figure 7: Unloading/loading stiffness ratio for longer/shorter AF 17×17 M5® samples.

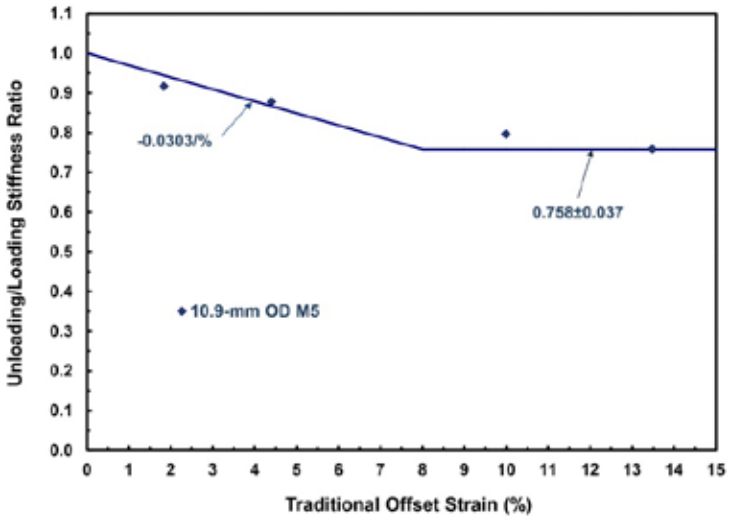

Figure 8: Unloading/loading stiffness ratio for larger-diameter AF 15×15 M5® samples.

The correlation shown in Fig. 6 is given by the following equation:

$$K_U/K_{LM} = 1 - 0.0303\ \delta_p/D_{mo} \text{ for } \delta_p/D_{mo} \le 8.0\% \quad (5a)$$

$$K_U/K_{LM} = 0.758 \text{ for } \delta_p/D_{mo} > 8.0\% \quad (5b)$$

There is reasonable confidence in using Eqs. 5a and 5b to calculate the corrected offset displacement (δ_{pc}) and corresponding corrected offset strain (δ_{pc}/ D_{mo}) for cladding rings that do not crack or do not experience minor cracking prior to a significant load drop. However, with the possible exception of HBU-fuel M5® with long radial hydrides, sparsely distributed circumferential hydrides, and a very thin oxide layer (≈10±3 μm), most HBU-fuel cladding samples exhibited some cracking prior to the maximum displacement or prior to a significant load drop. The effects of minor cracks (e.g., multiple cracks through the hydride rim extending 10% to 20% of the wall thickness) can reduce the unloading slope by as much as 25%. A large number of tests with HBU-fuel cladding would be needed to develop a correlation for unloading slope as a function of number and depth of cracks. These tests would have to be conducted at a slow enough displacement rate (e.g., 0.05 mm/s) in order to terminate the test before major cracking had occurred. The compressed rings would then have to subjected to metallographic examination to determine crack location, number, and depth. Until such tests are performed, uncertainty in the determination of the corrected offset strain has to be taken into account in the formulation of an embrittlement criterion. A set of criteria is described in the following.

The criteria for determining embrittlement remain the same for cladding with radial and circumferential hydrides: δ_{pc}/D_{mo} <2% prior to >25% load drop or >50% decrease in loading slope. In previous work [6–8], it was established that >25% load drop or >50% decrease in loading slope corresponds to a crack or cracks extending through >50% of the wall thickness. In a few cases, an "implied" load drop >25% is used. For these cases, cracking initiates at loads much less that the P_{max} measured for rings that do not exhibit early cracking. Although the explicit load drops appear to be <25% followed by a smooth load-displacement curve, the P_{max} may be 30% to 50% less than expected. Metallographic examination indicated extensive cracking for such samples.

The 2% offset strain limit is based on the uncertainty in the measurement of the permanent displacement (pre-test diameter minus post-test diameter equals d_p) for HBU-fuel cladding and the added uncertainty in the permanent displacement measurement for HBU-fuel cladding due to flaking off of the oxide layer under the applied loading plate and above the support plate. Multiple cracks through the oxide layer and the hydride rim lower the unloading stiffness to values less than shown in Fig. 6, which has also been factored into the 2% offset-strain limit. An additional consideration is that the material strain is less than the ring structural strain (i.e., permanent and corrected offset displacements normalized to the cladding outer diameter). As the HBU-fuel M5® tested had very thin oxide layers (10±3 μm) and no hydride rim, the 2% offset strain criterion is more conservative for this HBU-fuel alloy than for the HBU-fuel Zry-4 and ZIRLO™ samples tested, both of which had thicker oxide layers (30−100 μm) and thick hydride rims (30−100 μm).

Although Eqs. 5a and 5b are a better fit to benchmark test data than Eqs. 4a and 4b, the differences in unloading slope and offset displacement are negligible for low traditional offset strains. For 2% traditional offset strain, Eq. 5a predicts 0.94 for K_U/K_{LM} while Eq. 4a predicts 0.95 for K_U/K_{LM}. Therefore, use of the best-fit correlation (Eq. 5a) would have a negligible impact on the DTT, especially if the slope of the offset strain vs. test temperature is very steep. Equations 4a and 4b are used in the current work for determining K_U and corrected offset displacement. If the effects of minor cracking on the unloading slope can be included in a revised correlation or at least compensated for, a better correlation will be used to re-analyze past data sets and to analyze new data sets. This effort has been initiated (see Section 4).

3. PREVIOUS RESULTS FOR HBU-FUEL ZIRLO™ CLADDING

HBU-fuel ZIRLO™ was subjected to RCTs in the as-irradiated condition and following RHT at 350°C and 400°C PCT and 80–141 MPa peak cladding stresses. The hydrogen concentrations of the test samples ranged from about 350 wppm to 650 wppm. Ductility results are summarized in Fig. 9. In the as-irradiated condition HBU ZIRLO™ had relatively high ductility (6% to >11%) for tests conducted at RT displacement rates of 0.05 mm/s to 50 mm/s and at 5 mm/s and RT to 150°C. The hydrogen content of the as-irradiated cladding segment was 530±70 wppm. For 400°C PCT and 80-MPa peak RHT hoop stress, radial hydrides were short (9±4% radial hydride continuity factor [RHCF]) and ductility values were moderately high at RT and 60°C and high (>9%) at 90°C and 150°C [8,11]. Thus, for peak RHT conditions of 400°C and ≤80 MPa, the corresponding DTT would be <20°C. The two rodlets subjected to peak RHT conditions of 400°C and 111 MPa exhibited longer radial hydrides (32±13%) and a higher DTT value (122°C) [5,6]. For HBU ZIRLO™ rodlets subjected to peak RHT conditions of 350°C and 400°C within the narrow stress range of 87–89 MPa, radial hydrides remained relatively short (≤20% on average) and the DTT was <30°C. However, for rodlets subjected to higher peak hoop stresses (93–94 MPa at 350°C and 111 MPa at 400°C), radial hydrides were considerably longer (>30%) and the DTT values were >120°C. Excluding the influence of total hydrogen content, the results suggested a very high sensitivity of ZIRLO™ to radial-hydride-induced embrittlement within the narrow stress range of 90±3 MPa. This is shown in Fig. 10 in which the DTT is plotted as a function of peak hoop stress (solid symbols) and corresponding precipitation-temperature hoop stress (open symbols). However, the higher hydrogen content (644±172) and thicker hydride rim (≈66±11 μm) for the 350°C/94-MPa case may have contributed to its higher DTT value (≈140°C).

Additional test data are needed to confirm the high sensitivity of HBU ZIRLO™ DTT to RHT stress and to investigate the effects of very thick hydride rims on cladding ductility. In Section 4, RCTs are performed using as-irradiated HBU-fuel ZIRLO™ samples with thick hydride rims and high hydrogen content (≈650 wppm) to determine if the high concentration of circumferential hydrides leads to low ductility.

It is instructive to visualize the increase in lengths of radial hydrides with increasing peak RHT hoop stress. Figure 11 shows a partial cross section of the 400°C/80-MPa with only 7% RHCF. On the basis of multiple examinations of partial cross sections at several axial locations, the RHCF was only 9±4% and the extrapolated DTT was <20°C. Figure 12 shows a partial cross section of the rodlet subjected to 400°C/89-MPa with longer radial hydrides (19±9% for multiple cross sections at several axial locations), but the DTT was only about 20°C. This 400°C test was repeated using an adjacent cladding segment and the 3-temperature-cycle RHT condition. The peak hoop stress was 88-MPa. The temperature cycling (100°C/cycle) had no effect on the RHCF (18±7%) or the DTT (20°C). The increase of hoop stress to 111 MPa had a significant effect on radial hydride length (increased to 32±13%; see Fig. 13) and DTT (increased to 120°C). Figure 14 shows the effect of the highest RHT stress level (141 MPa at 400°C) tested: 65±17% RHCF and ≈185°C DTT. Subsequent tests were conducted for 350°C PCT. Figure 15 shows an image for the 350°C/87-MPa peak RHT condition. The RHCF dropped back to 19±10% and the DTT was 28°C, both of which indicate peak hoop stress had a stronger effect on results than the PCT. The last two images are for the 3-temperature-cycle RHT with 350°C/93-MPa (see Fig. 16) and the 1-cycle RHT at 350°C/94-MPa (see Fig. 17). The corresponding values for RHCF and DTT were 30±11% and 37±11% for RHCF and 125°C and ≈140°C for DTT.

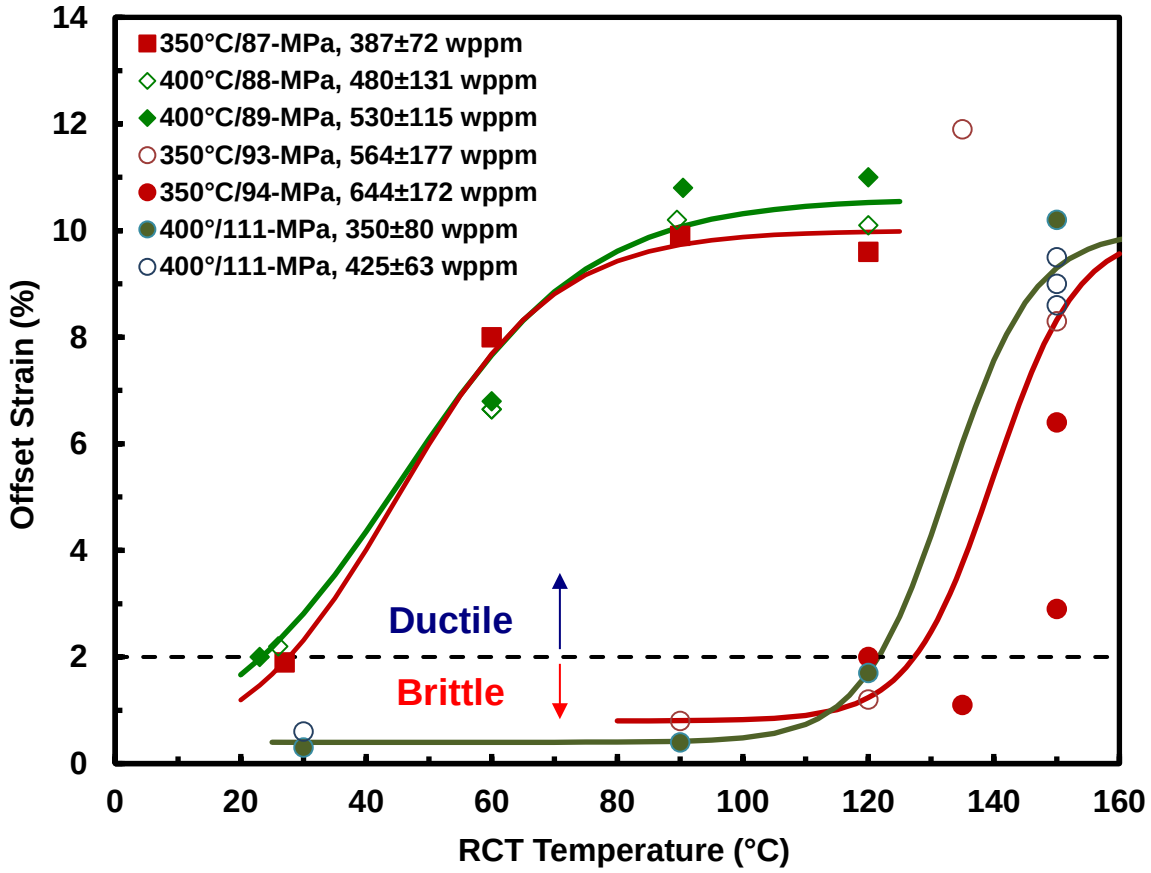

Figure 9: Summary of ductility data for HBU ZIRLO™ following RHT at 400°C and 350°C PCT.

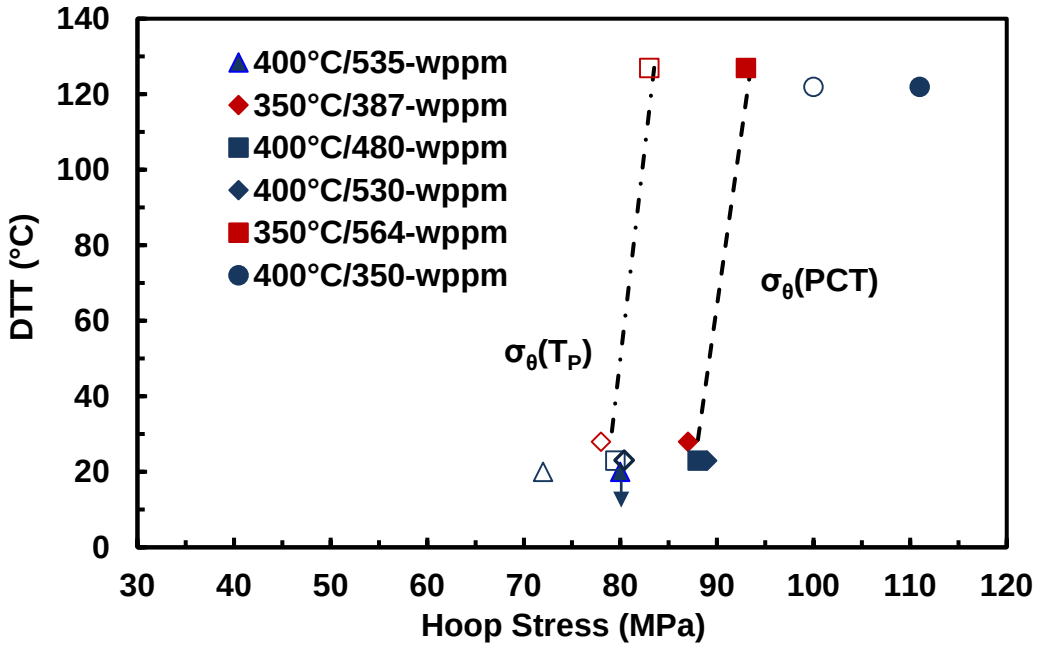

Figure 10: DTT vs. hoop stress for HBU ZIRLO™ following RHT at 400°C and 350°C PCT. Solid symbols are hoop stresses at PCT; open symbols are hoop stresses at T_P.

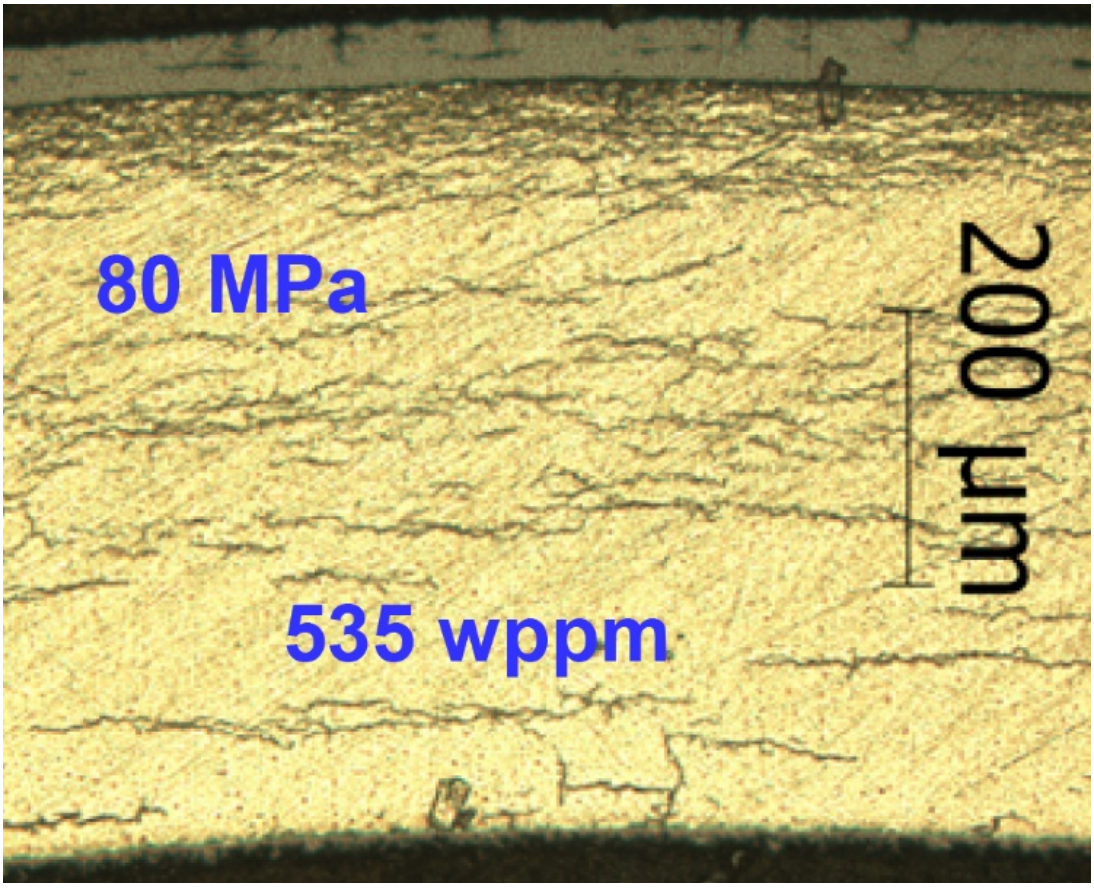

Figure 11: HBU-fuel ZIRLO™ following RHT at 400°C/80-MPa: 9±4% RHCF and <20°C DTT.

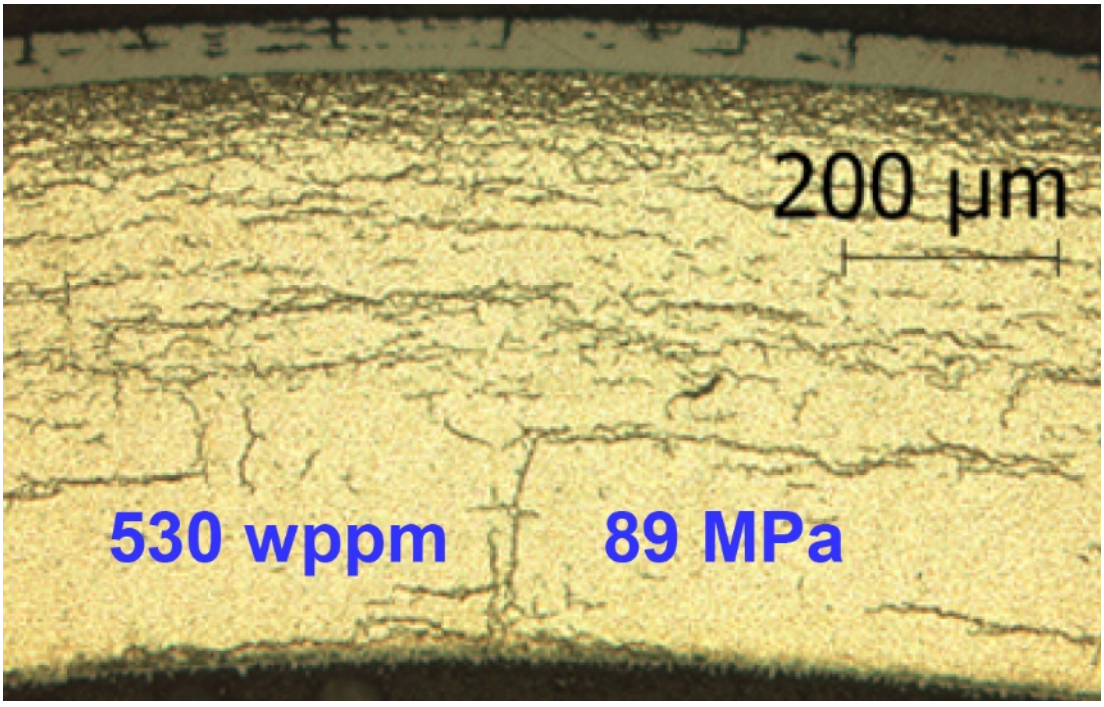

Figure 12: HBU-fuel ZIRLO™ following RHT at 400°C/89-MPa: 19±9% RHCF and 20°C DTT.

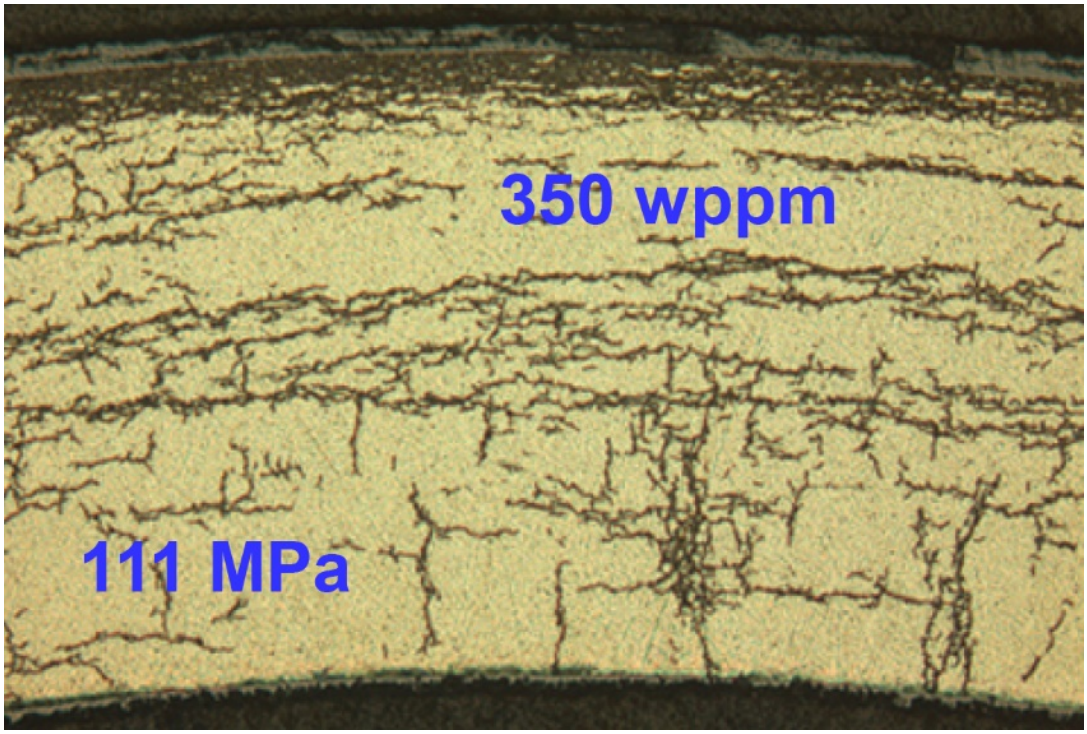

Figure 13: HBU-fuel ZIRLO™ following RHT at 400°C/111-MPa: 32±13% RHCF and 120°C DTT.

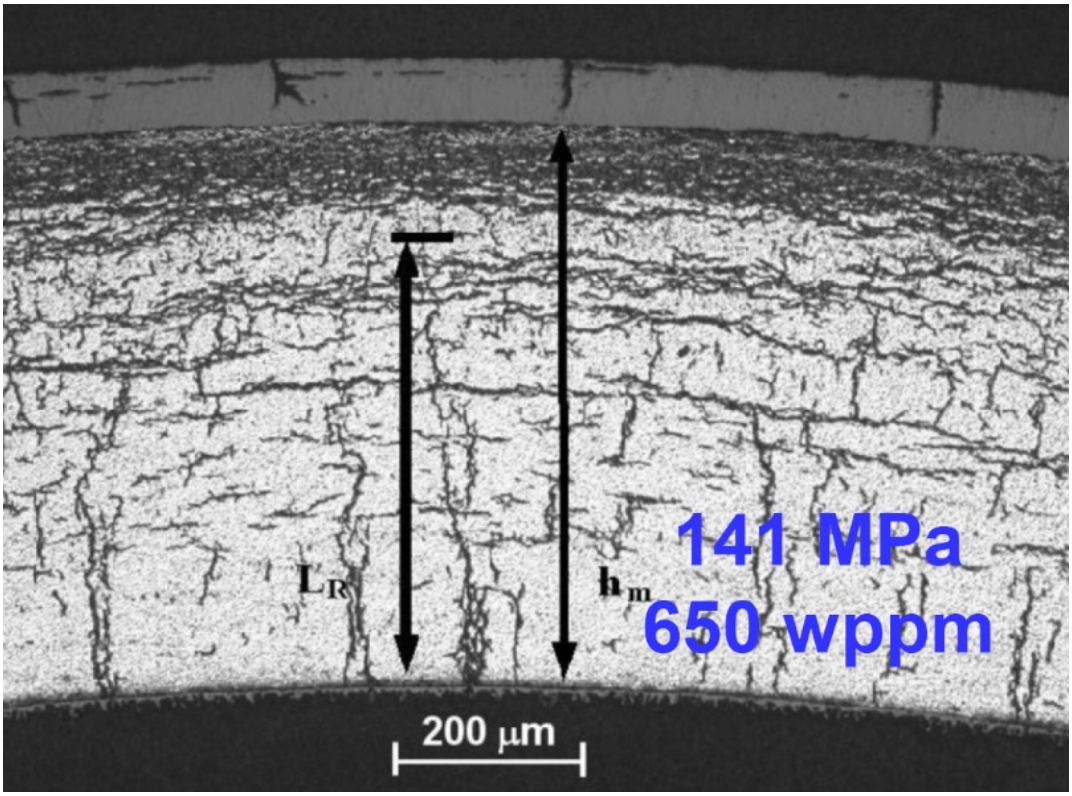

Figure 14: HBU-fuel ZIRLO™ following RHT at 400°C/141-MPa: 65±17% RHCF and ≈185°C DTT.

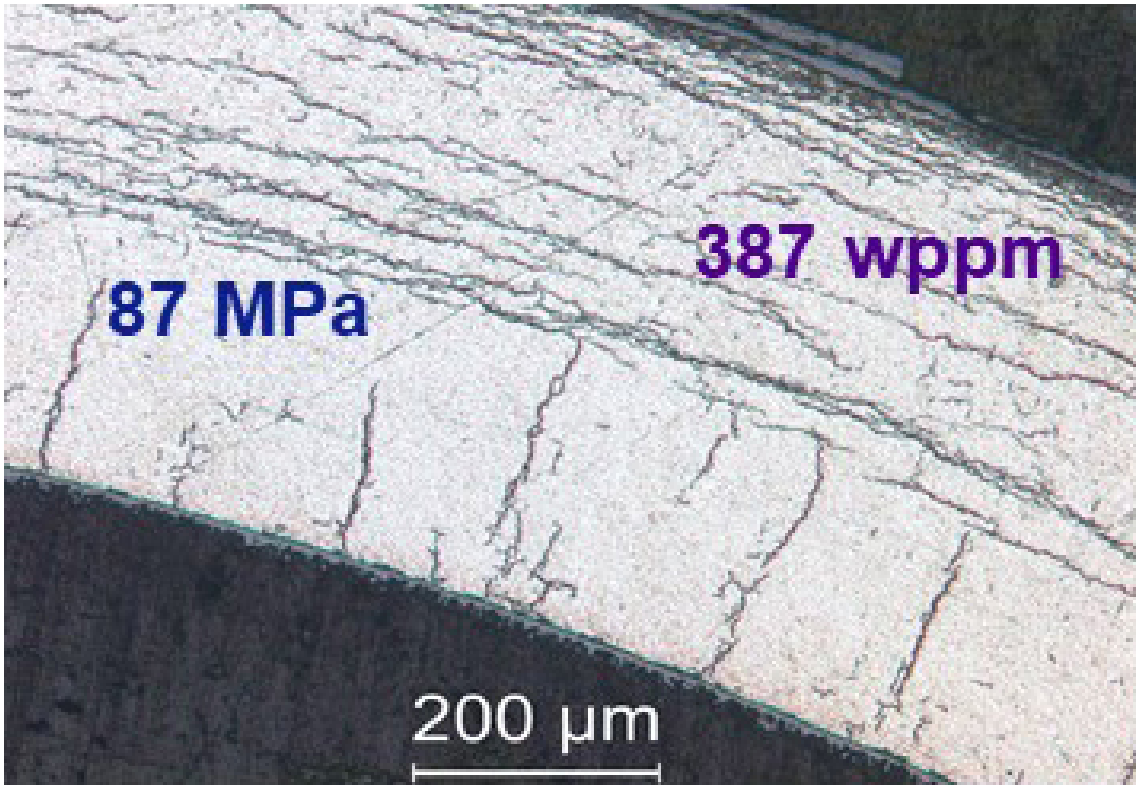

Figure 15: HBU-fuel ZIRLO™ following RHT at 350°C/87-MPa: 19±10% RHCF and 28°C DTT.

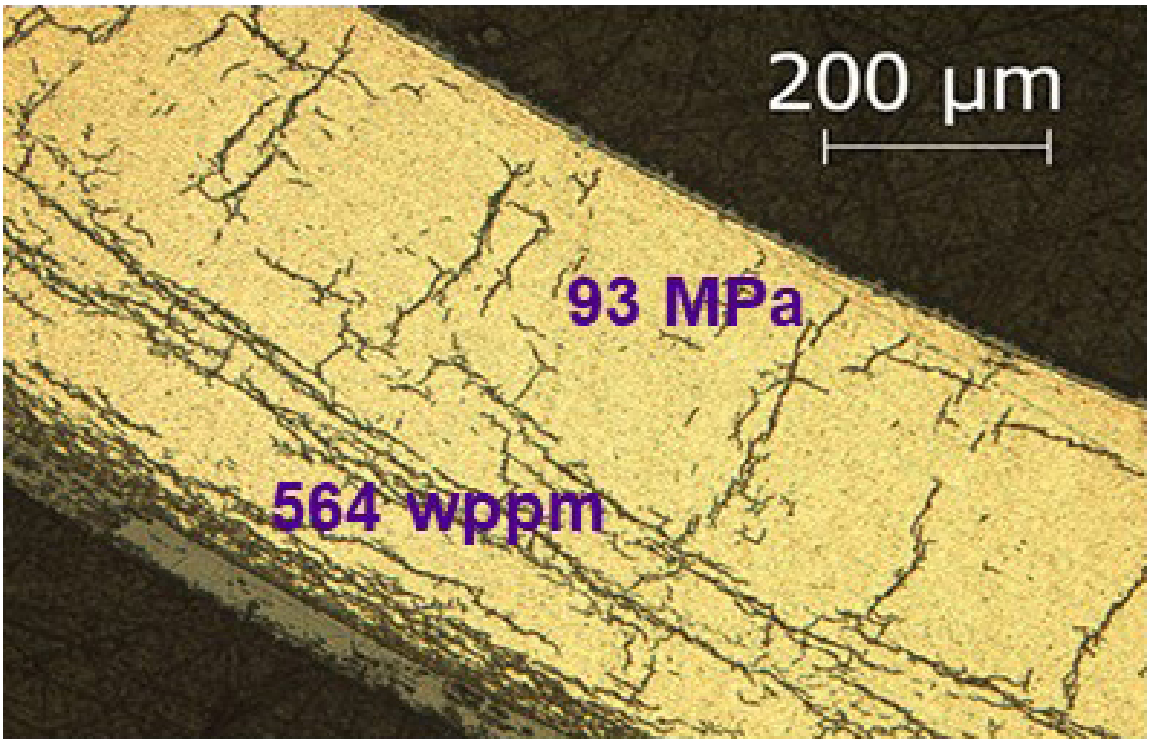

Figure 16: HBU-fuel ZIRLO™ following RHT at 350°C/93-MPa: 30±11% RHCF and ≈125°C DTT.

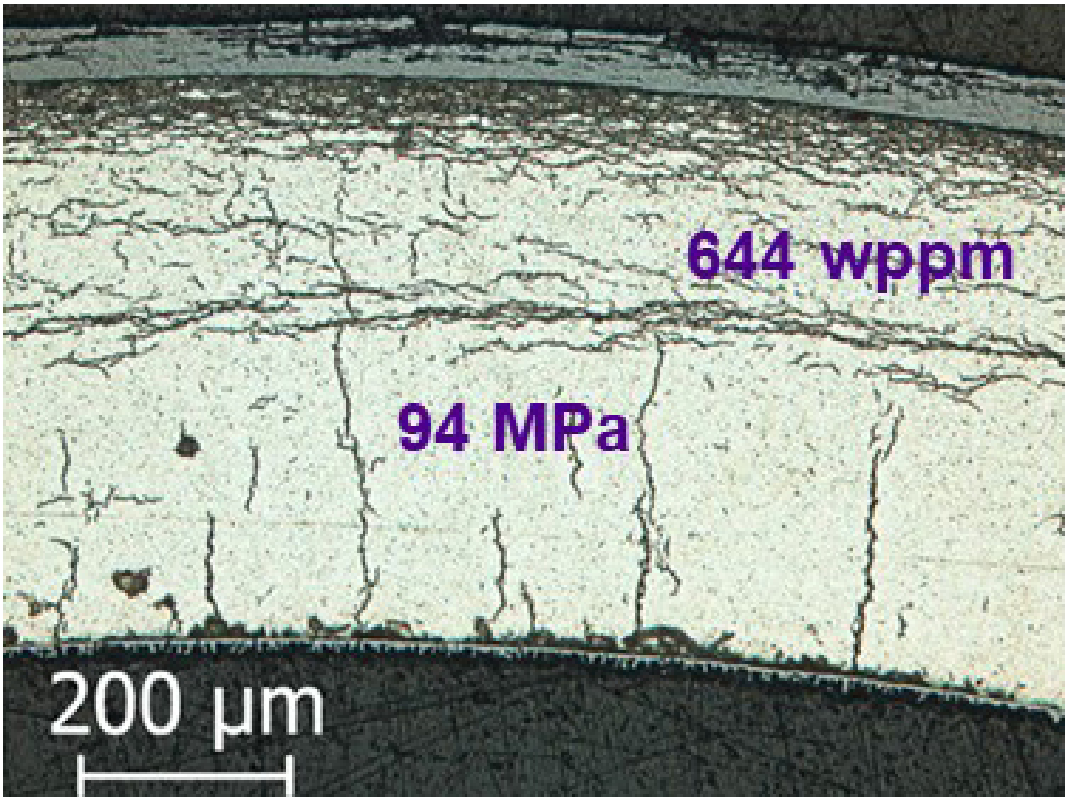

Figure 17: HBU-fuel ZIRLO™ following RHT at 350°C/94-MPa: 37±11% RHCF and ≈140°C DTT.

4. RESULTS FROM CURRENT TESTS

4.1 REVISED RESULTS FOR HBU-FUEL ZIRLO™ RODLET 646C

Rodlet 646C was tested in FY2017 and results were reported in Ref. 15. The rodlet was subjected to RHT with a 24-hour hold at 350°C followed by cooling at 5°C/h to 130°C. However, at some point during the RHT, the sample lost partial or total pressure as indicated by the absence of radial hydrides following RHT. The target peak hoop stress was 93 MPa, but the actual peak hoop stress was <70 MPa during cooling. Also, we were unable to measure hydrogen content due to failure of our LECO hydrogen analyzer, which will be replaced. However, the hydrogen content can be estimated by comparing oxide layer thickness values for 646C and 646D. The measured hydrogen content of 646D was 387±72 wppm. Segment 646C was adjacent to and just below segment 646D in the parent fuel rod. Table 2 shows the comparison between the two segments based on outer-diameter measurements and metallographic examinations for cross sections near the mid-span of each rodlet. As segment 646C is expected to have slightly lower hydrogen content than segment 646D, the estimated hydrogen content is 350 wppm.

Table 2 Characterization results for HBU-fuel ZIRLO™ rodlets 646C and 646D.

Parameter	Rodlet 346C	Rodlet 346D
Outer Diameter (D_o), mm	9.50	9.49
Oxide Layer Thickness (h_{ox}), µm	30±1	30±1
Metal Outer Diameter (D_{mo}), mm	9.44	9.43
Metal Wall Thickness (h_m), mm	0.56	0.56
Metal Inner Diameter (D_{mi}), mm	8.31	8.31
Hydrogen Content (C_H), wppm	≈350	387±72

Post-RCT metallographic examinations were performed during the current reporting period to aid in the interpretation of load-displacement curves. Figure 18 shows the updated sectioning diagram, which identifies post-RCT locations within 646C3 tested at 5 mm/s and 24°C and within 646C4 tested at 5 mm/s and 60°C for which metallographic examinations were performed. Load-displacement curves for both tests indicated steep load drops of 20% to 22%. The 24°C load-displacement curve indicated a second steep load drop near the maximum displacement. However, the percent load drop could not be determined accurately because the sample was unloaded at 5 mm/s close to this location. The purposes of the metallographic examinations were to determine number and extent of cracks associated with these load drops.

Figures 19 and 20 show images taken at the 3 o'clock and 9 o'clock positions (normal to the loading direction), respectively, for the 646C3B post-RCT surface, which was near the mid-span of the RCT sample. Cracking was quite severe at the 3 o'clock orientation with only a thin ligament of cladding that remained intact. Cracking initiated in the outer surface of the cladding ring, propagated essentially radially through 30% of the cladding wall and then along a circumferential hydride before an additional radial crack formed that extended through about 38% of the cladding wall. A couple of short radial cracks (<14% of the cladding wall) were observed in the hydride rim and one radial crack (25% of the cladding wall) was observed at the cladding inner surface.

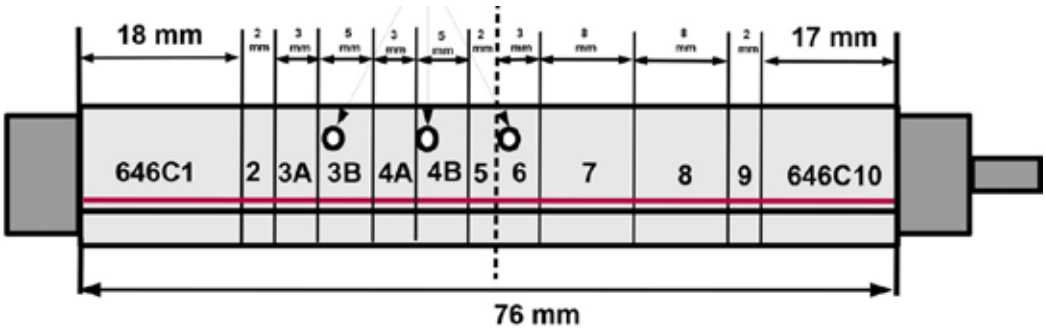

Figure 18: Revised sectioning diagram for HBU-fuel ZIRLO™ rodlet 646C.

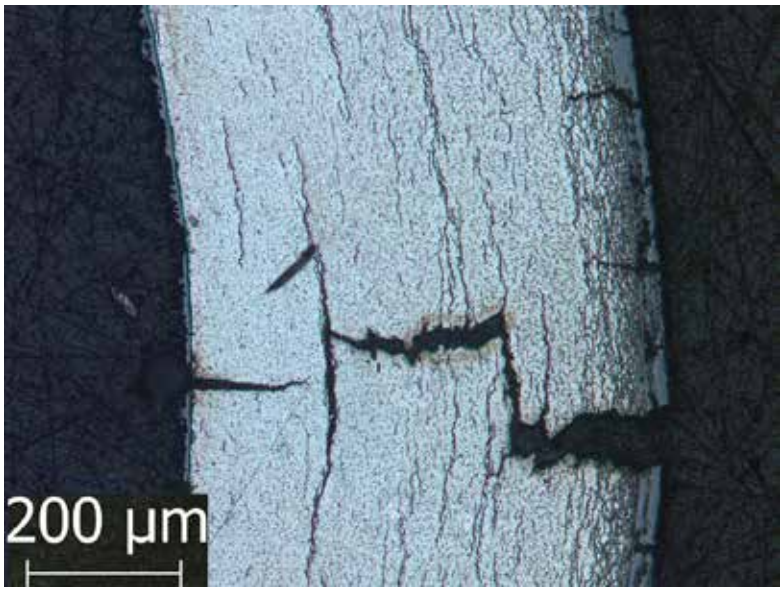

Figure 19: Metallographic image of post-RCT 646C3B at the 3 o'clock position.

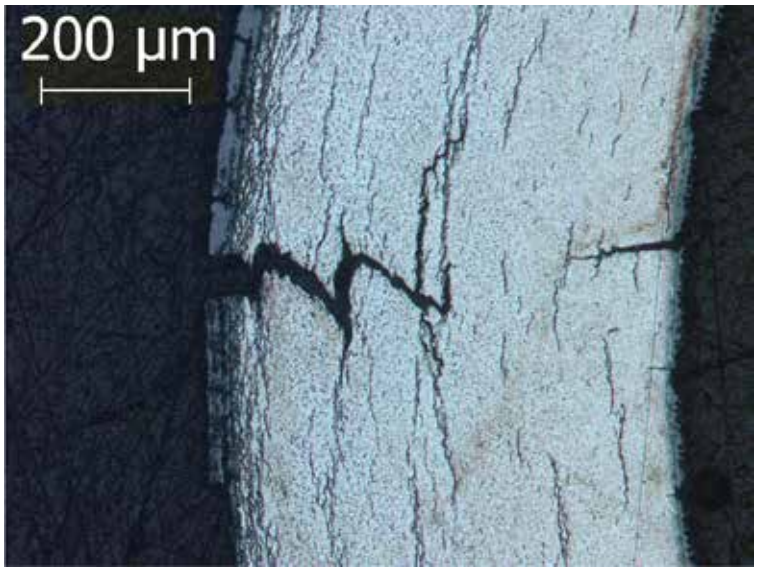

Figure 20: Metallographic image of post-RCT 646C3B at the 9 o'clock position.

The extensive cracking observed in the 646C3B cross section suggests that there were two major load drops. However, to learn about the progression of the cracks, especially after the first load drop, one would have to conduct the test at a slower displacement rate (e.g., 0.05 mm/s) and stop the test immediately after the first load drop. The load-displacement curve for the 656C3 RCT is shown in Fig. 21. Although the first load drop (22%) is slightly less than the 25% criterion indicating a crack extending through >50% of the cladding wall, the assumption is made that crack extension was ≥50% after the first load drop. The 5.1% corrected offset strain is determined by the red unloading slope starting at the peak load (616 N).

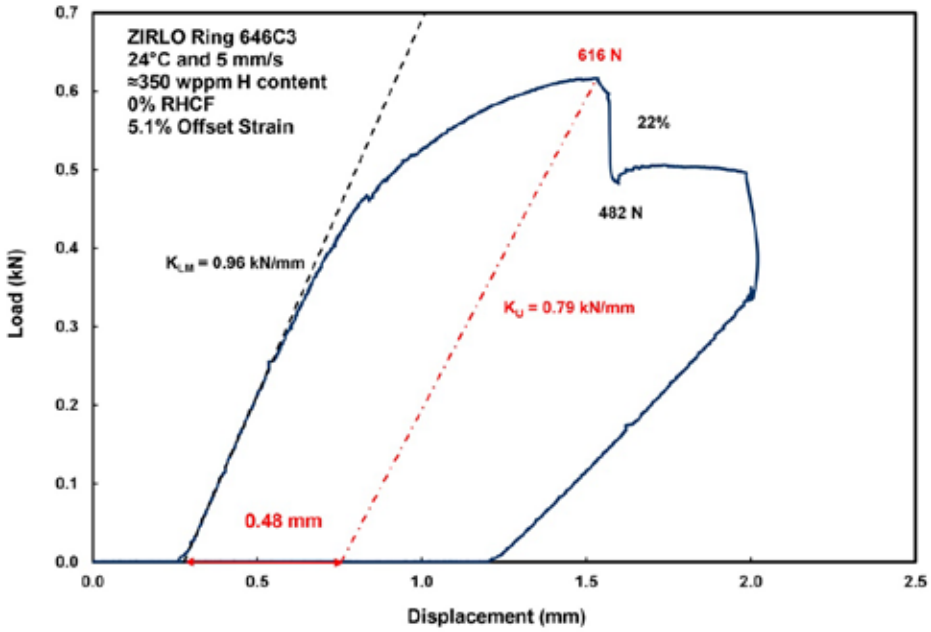

Figure 21: Load-displacement curve for 646C3 tested at 24°C and 5 mm/s.

Ring 646C4 was tested at 60°C and 5 mm/s displacement rate. The sample experienced a single load drop of about 20%. Crack growth is assumed to have occurred during this load drop with no extension during the small remaining displacement at lower load. Metallographic examination revealed cracking at the 9 o'clock orientation only. As shown in Fig. 22, the crack initiated in the hydride rim and proceeded through about 50% of the wall. A radial crack (about 22% of the cladding wall) was also observed at the cladding inner surface. It is not clear if the radial cracks observed for both samples are due to isolated, short radial hydrides observed in as-irradiated HBU-fuel ZIRLO™ (see subsection 4.2) or stress concentrations from substantial wall cracking.

Figure 23 shows the load displacement curve for the 646C4 sample tested at 60°C and 5 mm/s. The red dashed line represents the unloading slope from 591 N, which gives a corrected offset strain of 6.5%. Tests conducted at 90°C (see Fig. 24) and 120°C (see Fig. 25) did not exhibit significant load drops. Rather gradual load drops were observed: 8% for the 90°C test and 10% for the 120°C test. Previous work established that these small and gradual load drops were caused by short cracks through the hydride rim and along circumferential hydrides at the 3 o'clock and 9 o'clock orientations. The corrected offset strains (9.9% and 10.7%) were close to the measured permanent strains (9.3% and 10.5%). As the correlation for determining the unloading slope does not account for cracking, it can be surmised that cracking was minor in terms of depth and limited in number of cracks.

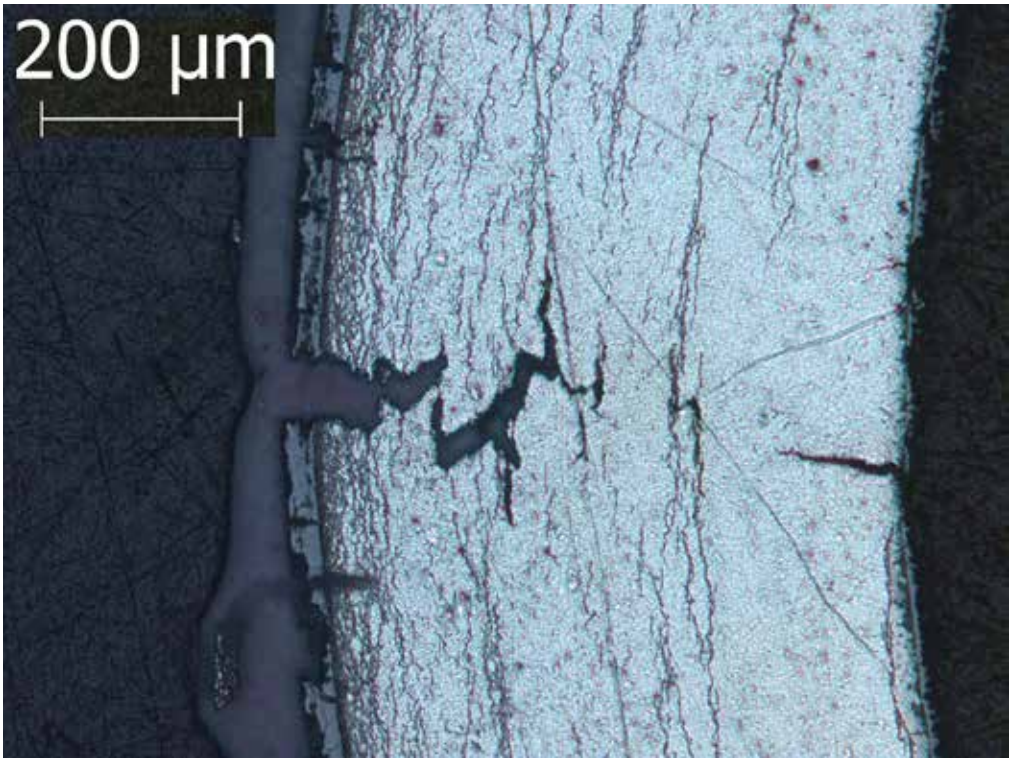

Figure 22: Metallographic image of post-RCT 646C4B at the 9 o'clock position.

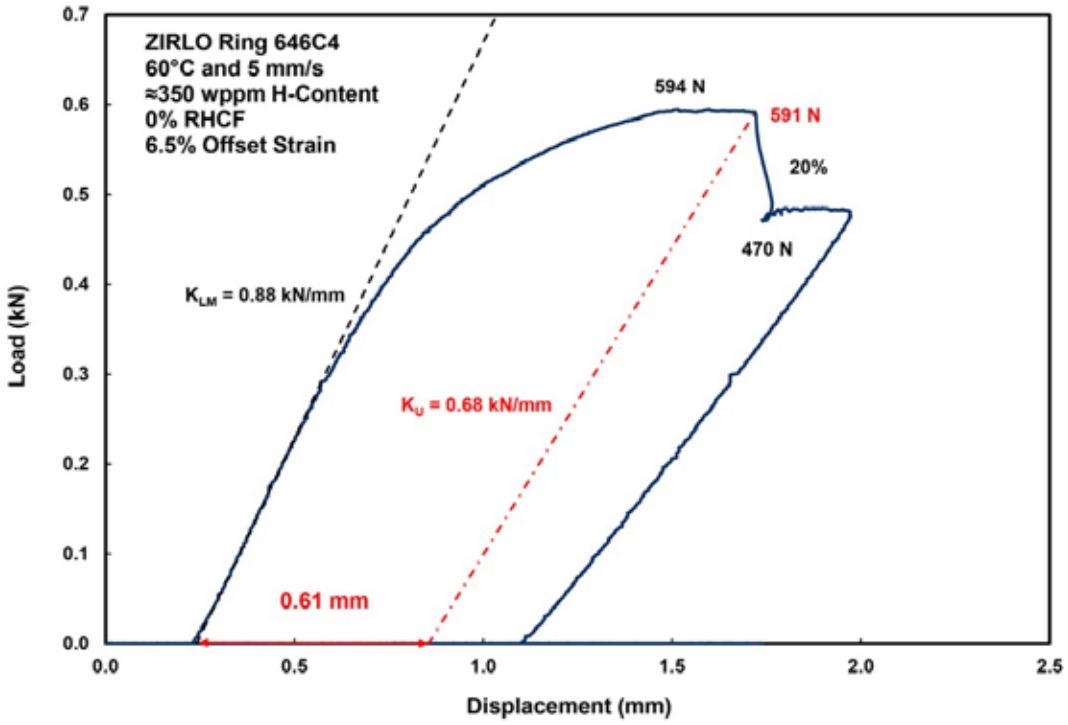

Figure 23: Load-displacement curve for 646C4 tested at 60°C and 5 mm/s.

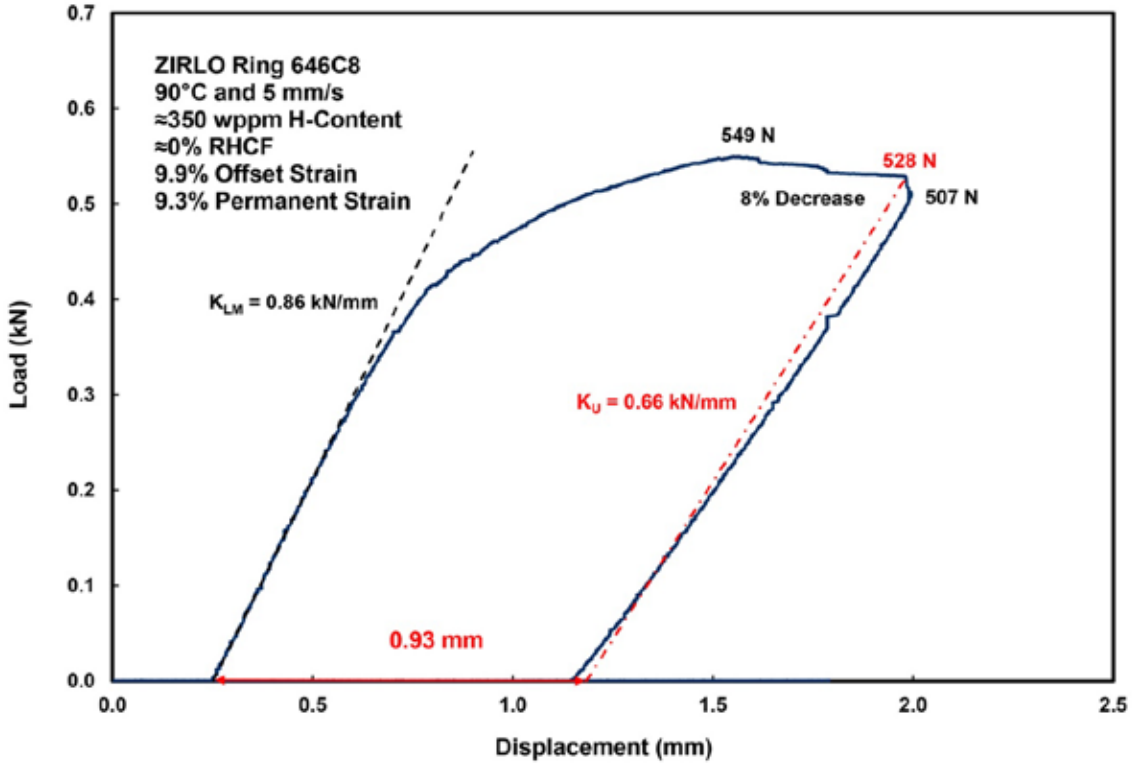

Figure 24: Load-displacement curve for 646C8 tested at 90°C and 5 mm/s.

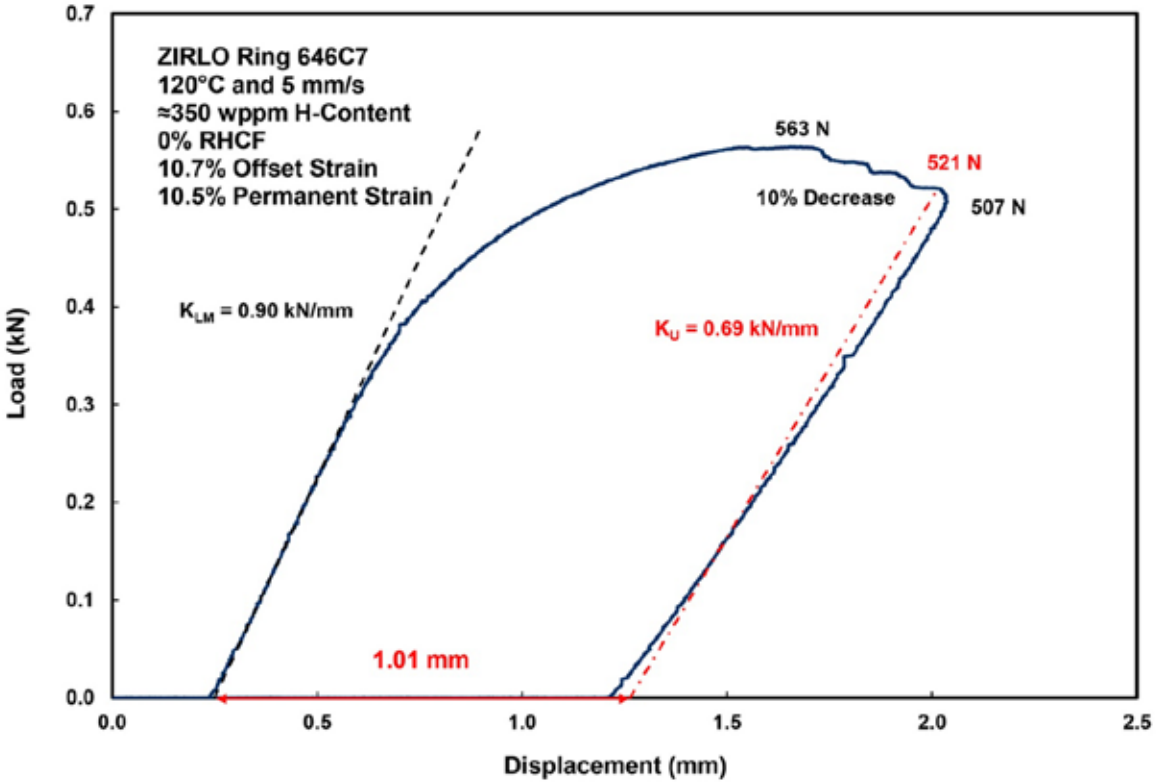

Figure 25: Load-displacement curve for 646C7 tested at 120°C and 5 mm/s.

4.2 RESULTS FOR HBU-FUEL ZIRLO™ SEGMENT 105G

Segment 105G was adjacent to and just above segment 105F, which was characterized and tested in FY2015. The hydrogen content for 105G was expected to be similar to what was measured for 105F: 644±172 wppm. The test plan called for rodlet fabrication and RT pressurization to give a peak hoop stress of 80–87 MPa at 350°C PCT. If the sample exhibited ductility at <30°C, then the narrow stress range of 90±3 MPa for ductility degradation and DTT increase would essentially be confirmed. However, during circumferential welding using the Astro Arc welder, the welder head stopped rotating around the sample after about 20 turns. Attempts to diagnose the problem and repair the welder head inside the glove box were unsuccessful. It was confirmed that the power supply to the welder head, which is outside the glove box, was working properly. A new welder head was ordered and will arrive during the first week of October 2018. The new welder-head/power-supply will be tested out of the glove box. Given the many parameters that need to be adjusted to get a good weld, ten successful welds with as-fabricated ZIRLO™ cladding and the new end-fixture design are required before the new welder head will be installed into the glove box. Following installation, a minimum of three successful as-fabricated ZIRLO™ rodlets need to be fabricated before using the new equipment for HBU-fuel cladding samples.

However, ductility data for the high-hydrogen-content 105G segment are valuable to assure that high-hydrogen-content ZIRLO™ has adequate ductility in the as-irradiated condition. Previous baseline studies of as-irradiated ZIRLO™ were conducted with a sample containing about 530-wppm hydrogen. Demonstration of adequate ductility for 105G would strongly indicate that the embrittlement exhibited by 105F was primarily due to radial hydrides rather than the high-hydrogen content of the sample.

Figure 26 shows the sectioning diagram for HBU-fuel ZIRLO™ segment 105G. Sample 105G4 was used for metallographic examination. Prior to sectioning, the outer diameter of the segment was measured at three axial locations and two orientations. Following sectioning and metallographic-mount preparation, the as-polished sample was examined at 100X magnification to determine cladding wall thickness and at 500X magnification to determine oxide layer thickness. Thirteen circumferential locations were used in this evaluation. The sample surface was then etched to image hydrides and estimate the hydride rim thickness. The comparison of characterization results for 105G and 105F is given in Table 3. On the basis of these results, the hydrogen content of 105G was estimated to be ≈650 wppm.

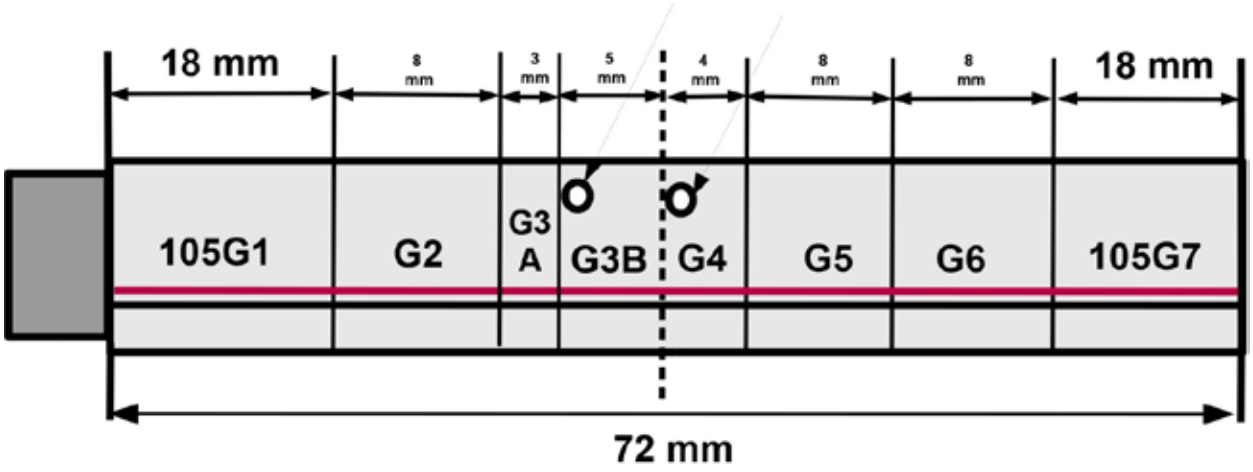

Figure 26: Sectioning diagram for HBU-fuel ZIRLO™ rodlet 105G.

Table 3 Characterization results for HBU-fuel ZIRLO™ segment 105G and rodlet 105F.

Parameter	Segment 105G	Rodlet 105F
Outer Diameter (D_o), mm	9.55	9.55
Oxide Layer Thickness (h_{ox}), µm	59±1	58±3
Metal Outer Diameter (D_{mo}), mm	9.43	9.43
Metal Wall Thickness (h_m), mm	0.55	0.55
Metal Inner Diameter (D_{mi}), mm	8.34	8.34
Hydride Rim Thickness, µm	≈73±18	≈66±11
Hydrogen Content (C_H), wppm	≈650	644±172

Metallographic images are shown at the 3 o'clock position (Fig. 27) and 6 o'clock position (Fig. 28), which represent regions of maximum and minimum hydride rim thickness, respectively.

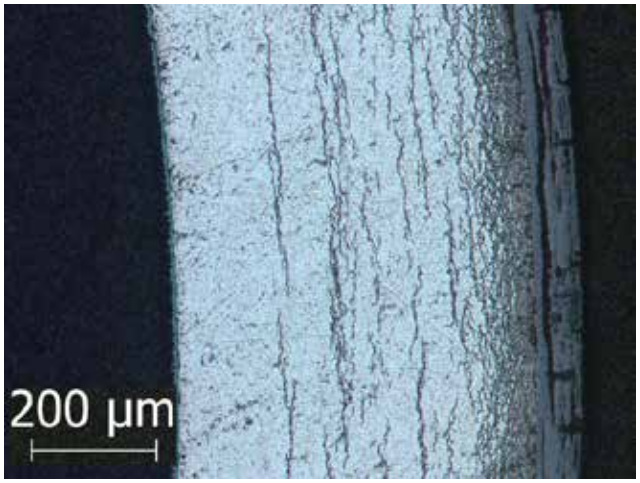

Figure 27: Metallographic image of 105G4 at the 3 o'clock position.

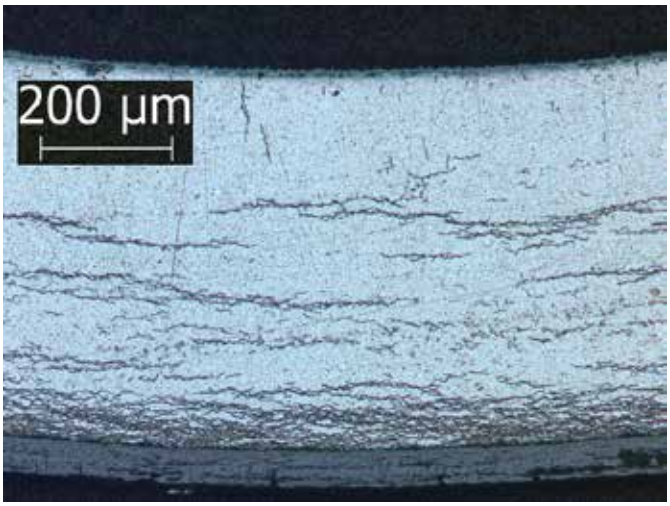

Figure 28: Metallographic image of 105G4 at the 6 o'clock position.

At the 3 o'clock position, the hydrides were all circumferential, the hydride rim was relatively thick and dense, and circumferential hydrides were relatively sparse within the inner two-thirds of the cladding wall. The circumferential hydrides were similar at the 6 o'clock position except that the hydride rim was thinner. It is interesting to note the presence of isolated radial hydrides near the cladding inner surface. These were observed at several positions, and they have been observed previously in the HBU-fuel ZIRLO™ cladding, as well as HBU-fuel M5® cladding, characterized at Argonne [7,8]. Radial hydrides likely precipitate during cooling from full to zero power and during reactor-refueling shutdown due to localized pellet-cladding mechanical interaction (PCMI) and/or due to residual stresses from localized PCMI at full power operation.

Ring 105G2 was subjected to a RCT at RT and 5 mm/s. Although it was clear that the sample exhibited intermediate ductility, gradual and stepped load drops made it difficult to determine how much ductility. In order to improve quantitative analysis for ductility (i.e., offset strain), a second RT test with sample 105C3 was conducted at 0.05 mm/s and terminated after a 26% load drop. Prior to conducting this test, the ring was rotated 90° relative to the loading direction. The permanent displacement, which included both plastic and crack displacement, was 0.63 mm and the corresponding permanent strain was 6.7%. Metallographic examination revealed a dominant crack (47–67% of the cladding wall) at the 9 o'clock position (Fig. 29) and a lesser crack (27% of cladding wall) at the 3 o'clock position (Fig. 30). Considering that this test was terminated after a single load drop, formation of these cracks occurred essentially simultaneously. The load-displacement curve for 105G3 is shown in Fig. 31.

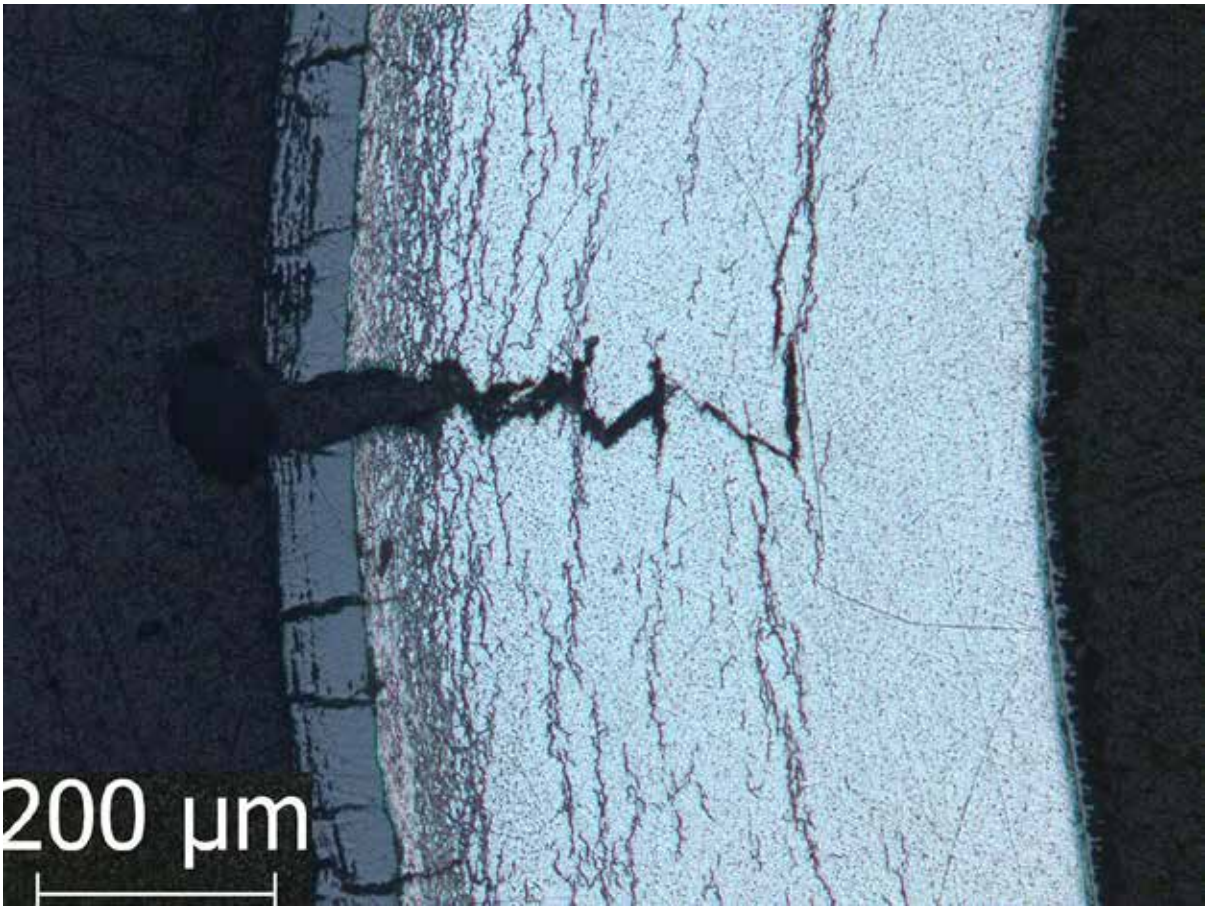

Figure 29: Metallographic image of 105G3 at the 9 o'clock position.

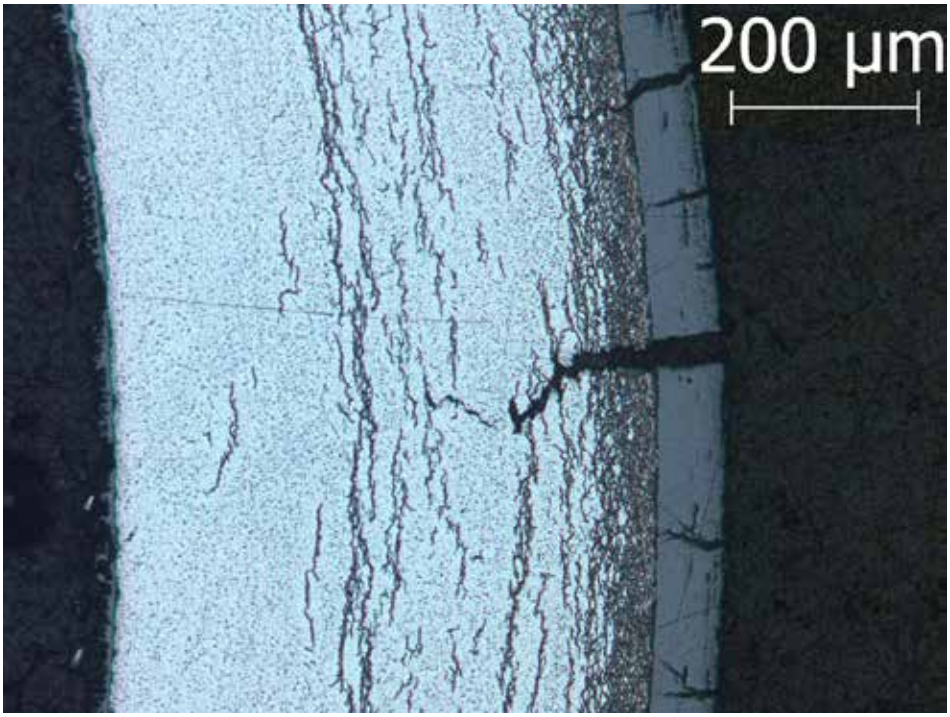

Figure 30: Metallographic image of 105G3 at the 3 o'clock position.

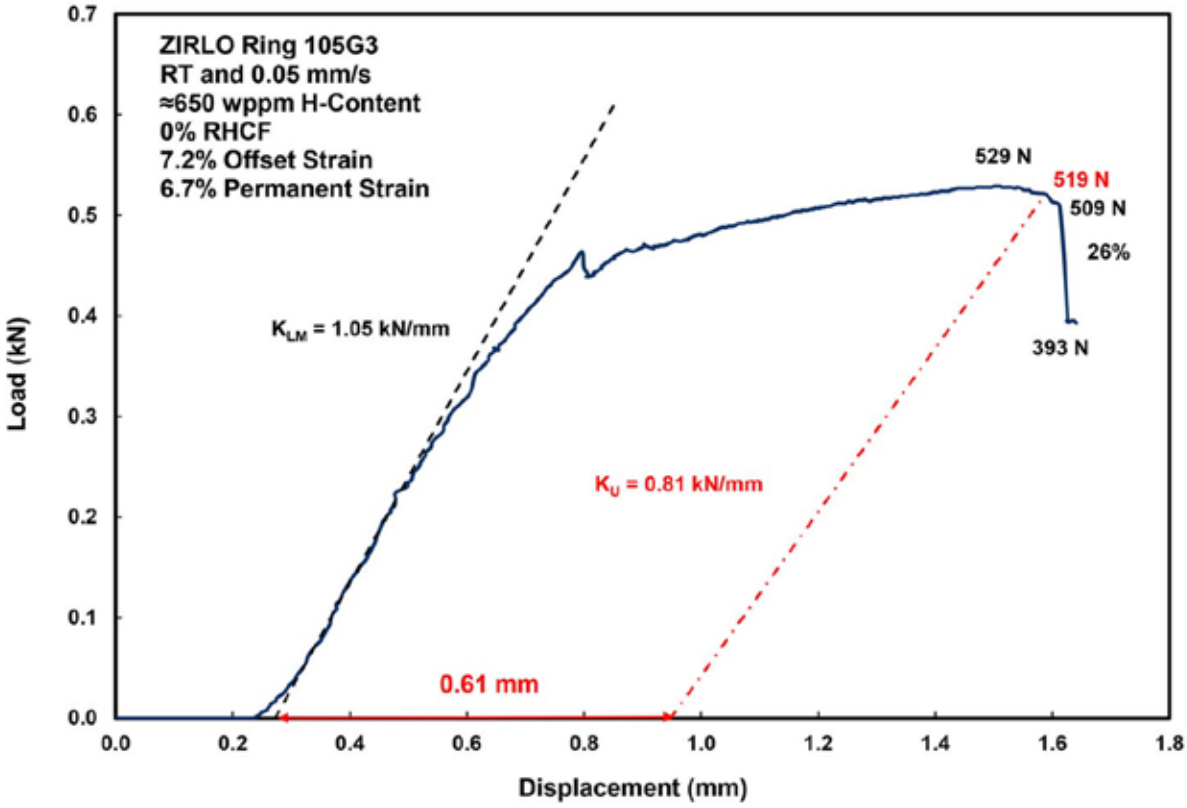

Figure 31: Load-displacement curve for 105G3 tested at RT and 0.05 mm/s.

Unloading to determine offset displacement was performed at the maximum load (529 N), at the minimum load (509 N) prior to the sharp load drop and at the intermediate load of 519 N. The red unloading line starting at 519 N gave the closest result to the measured offset displacement. The corresponding offset strain was 7.2%. These results suggest, but do not prove, that for a gradual load drop followed by a steep load drop, unloading at the average load during the gradual load drop partially compensates for the decrease in unloading slope that is not included in the correlations (Eqs. 4 and 5) for unloading slope. The small load drop at about 0.7-mm displacement should be ignored. It was an artifact of the Instron 8511, which was also observed in benchmark testing, at the slow displacement rate. This approach for determining the load for unloading was adopted in the analysis of the three other load-displacement curves for tests conducted at 5 mm/s and temperatures of RT, 90°C and 120°C. All of these samples had the same orientation as 105G3 relative to the loading direction. Figures 32, 33, and 34, respectively, show the load-displacement curves and offset strain results for these three tests. While it worked well for these three cases, the approach to dealing with a gradual load drop needs to be validated by applying it to the large database generated previously.

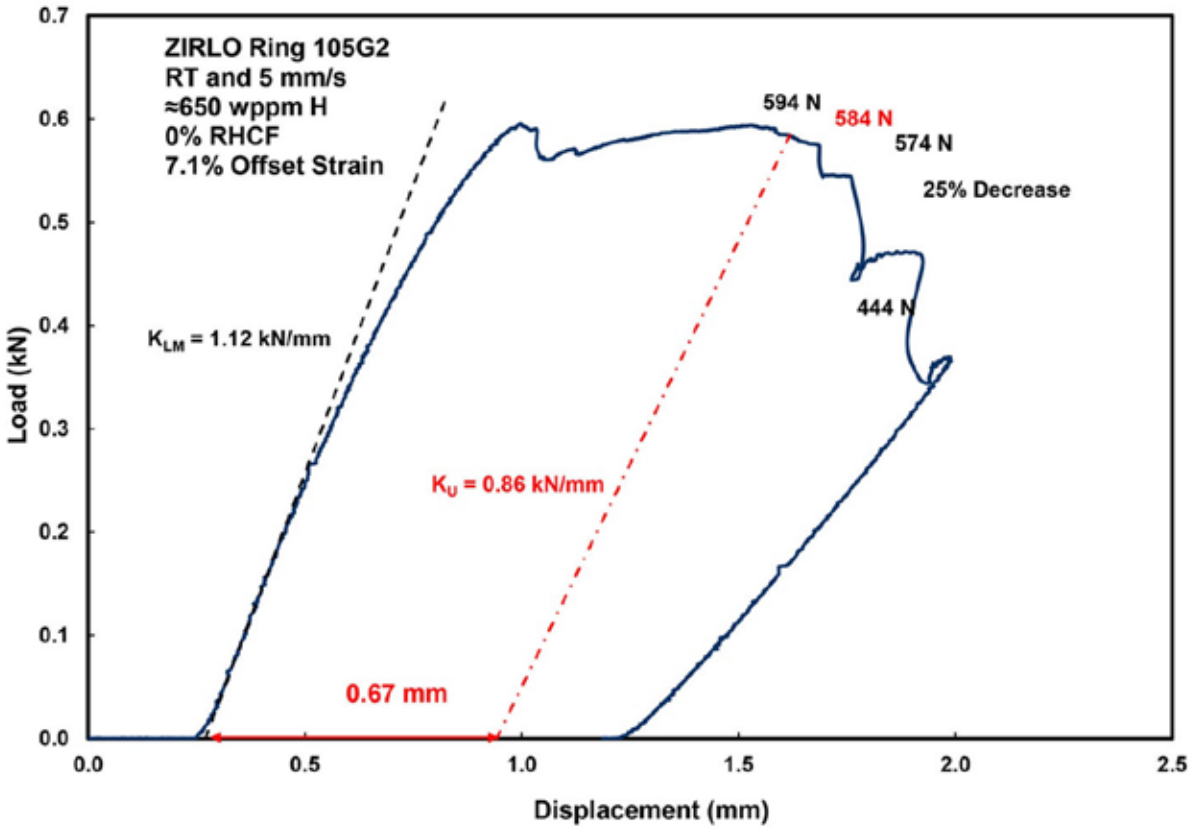

Figure 32: Load-displacement curve for 105G2 tested at RT and 5 mm/s.

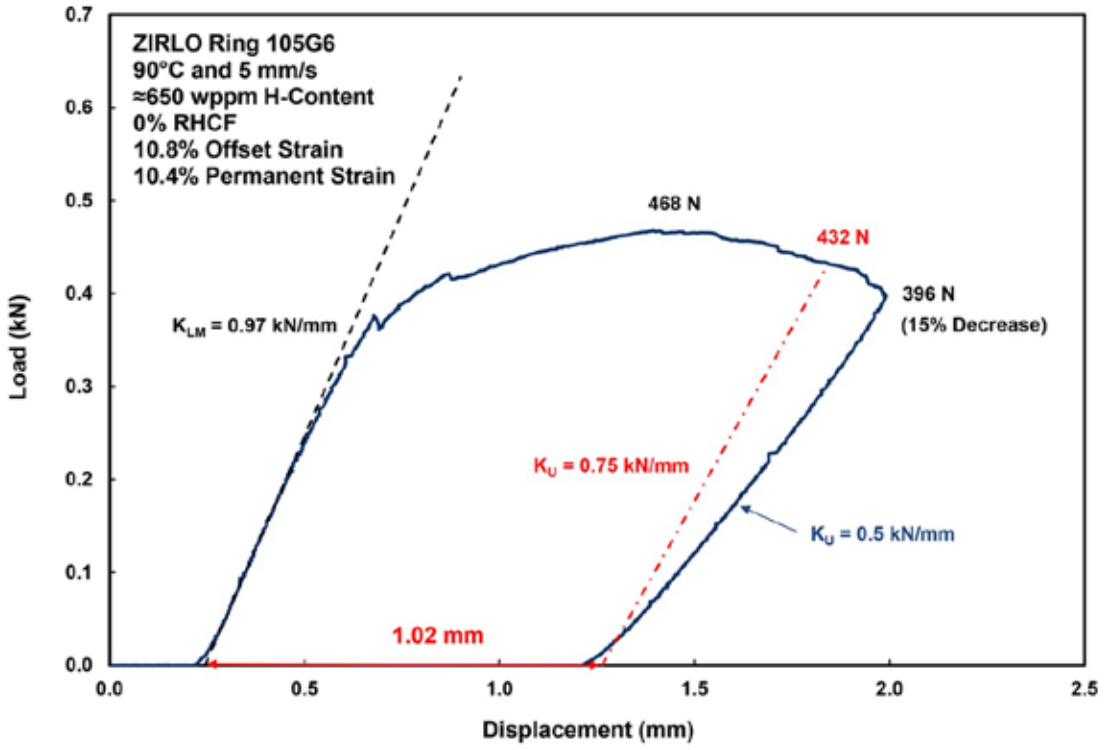

Figure 33: Load-displacement curve for 105G6 tested at 90°C and 5 mm/s.

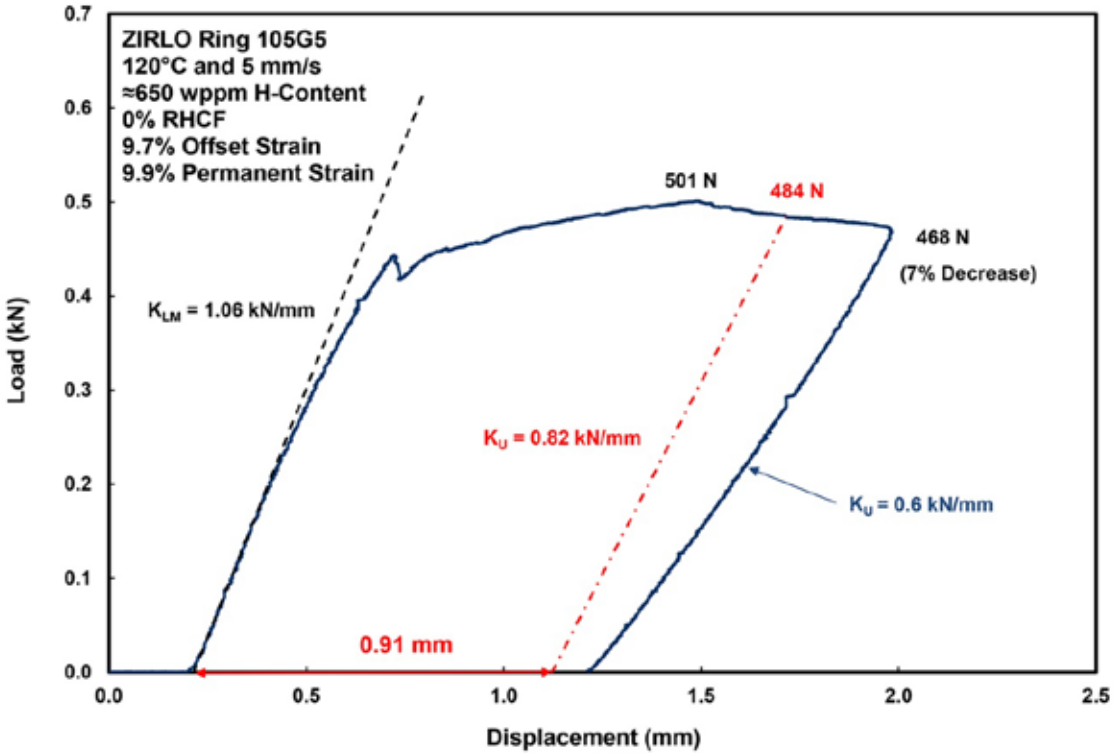

Figure 34: Load-displacement curve for 105G5 tested at 120°C and 5 mm/s.

Page intentionally blank

5. DISCUSSION AND SUMMARY

Ductility of As-irradiated HBU-fuel ZIRLO™ with High Hydrogen Content

The ductility (i.e., corrected offset strain) of as-irradiated HBU-fuel ZIRLO™ segment 105G with ≈650 wppm hydrogen was about 7% at RT and 10-11% at test temperatures of 90°C and 120°C. The load-displacement curves for the 90°C and 120°C exhibited signs of minor cracking during the 1.7-mm displacement. Permanent strains measured for these two samples were in excellent agreement with the corrected offset strains. These results are comparable to ductility values for samples from HBU-fuel ZIRLO™ rodlet 646C with only ≈350 wppm hydrogen: 5% at RT, 7% at 60°C, 10–11% at 90°C and 120°C. The distribution of circumferential hydrides across the cladding wall is a major factor in the higher-than-expected ductility. The ZIRLO™ used in the Argonne test program came from fuel rods irradiated at relatively high power, especially during the 4th cycle, in the North Anna reactors. Such high power and large temperature gradient across the cladding result in a very dense hydride rim with a small fraction of the total hydrogen below this rim. Baseline studies [8] revealed that for ZIRLO™ with 530±70 wppm hydrogen, only 136±7 wppm was in the inner two-thirds of the cladding wall. This pattern appears to apply to all the ZIRLO™ tested with 350–650 wppm hydrogen: as the hydrogen content increased, the hydride rim thickness increased with relatively little change in the hydrogen content below the hydride rim. This is in contrast to the ductility results for Zry-4 from fuel rods irradiated in the H.B. Robinson reactor at relatively low power and temperature gradient across the cladding wall. For the as-irradiated HBU-fuel Zry-4 used in the baseline study, the total hydrogen content was 640±140 wppm and the hydrogen content within the inner two-thirds of the cladding was 246±29 wppm. The Zry-4 with the more "diffuse" distribution of circumferential hydrides exhibited cracking at relatively low displacement.

However, the current results for ZIRLO™ with ≈650 wppm are significant in demonstrating that the low ductility and high DTT exhibited by companion sample 105F after slow cooling from 350°C/94-MPa were due primarily to the long radial hydrides (37±11%) that precipitated rather than the thick hydride rim.

The 2% Offset Strain Criterion

There has been much discussion regarding the 2% offset-strain criterion. RCT samples that exhibit ≥2% offset strain are classified as ductile and those with <2% offset strain are classified as brittle. The offset strains determined from load-displacement curves are values that have been corrected for the decrease in unloading slope with the increase in displacement beyond the elastic range. We start with ≤1% uncertainty in permanent displacement due to measurement error and spalling of the oxide layers in contact with the loading and support plates. Obviously this value is <1% for HBU-fuel M5® for which the oxide layer is relatively thin (10±3 μm). The determination of offset displacement and strain from load-displacement curves has two major uncertainties: (a) the decrease in unloading stiffness with minor cracking leading to a sharp, significant load drop (>25%) and (b) the further decrease in unloading stiffness following intermediate load drops of 10% to 20%. An additional uncertainty of 1% beyond the 1% permanent strain uncertainty is included in the ductility criterion to account for these two effects. The 2% criterion is likely conservative for HBU-fuel M5®, which has a thin oxide layer and no hydride rim. The case can be made that a lower transition strain (between 1% and 2%) can be used for HBU-fuel M5®. However, for steep ductility decrease with decreasing test temperature, lowering the 2% criterion to a 1% criterion would have only a small effect on the DTT. Until improvements are made and validated to account for minor and intermediate cracking in the unloading-stiffness correlation, the proper way to interpret and use the 2% criterion is: (a) for corrected offset strains ≥2% there is high confidence that the material has retained ductility; (b) for corrected offset strains between 1% and <2% there is high

uncertainty regarding ductility retention and (c) for corrected offset strains <1% there is high confidence that the material behaves in a brittle manner in response to hoop-stress loading. Improvements in determining the load to use for unloading and the unloading slope are discussed in the next section.

Unloading Slope and Relevant Load for Unloading

The corrected offset strains derived from load-displacement curves depend on the point along the curve at which unloading should be performed and the unloading slope. Benchmark tests conducted in the current work, along with those reported previously, have been used to establish a validated relationship between the unloading slope ratio (K_U/K_{LM}) and the traditional offset strain (δ_p/D_{mo}). In particular, this correlation was shown to apply to larger diameter (10.9 mm vs. 9.5 mm) cladding, to shorter (6 mm) and longer (10 mm) cladding rings, and to wall thickness values in the range of 0.57–0.63 mm. The data are relatively independent of displacement rates in the range of 0.05–50 mm/s and temperatures in the range of 20–150°C. The benchmark data and unloading-stiffness correlation are also consistent with RCT data for nine HBU-fuel M5® samples which were subjected to a wide range of test conditions without exhibiting any signs of cracking.

The remaining uncertainty in determining the unloading slope is the effects of minor cracking (e.g., multiple cracks through the hydride rim) on the further reduction in unloading slope. Such cracking results in a gradual decrease in load prior to the physical machine unloading or prior to a steep load drop indicating >50% wall cracking. The RCT results for HBU-fuel ZIRLO™ were used to determine how to compensate for use of an unloading slope that does not include the effects of minor cracks. Let P_{max} be the peak load and P_1 be the load at the beginning of a very sharp load drop. It has been shown for 105G samples that unloading from the point along the curve at the average of these two loads, $(P_{max} + P_1)/2$, resulted in excellent agreement between the corrected offset strain and the measured permanent strain. This approach will be used to reanalyze previous load-displacement curves that exhibited a gradual load drop before unloading or before a steep, significant crack.

Relevant Ranges of Internal Pressures and Hoop Stresses

ANL and other DOE Laboratories have been working with the Electric Power Research Institute (EPRI), fuel vendors, cask vendors, and the international community to determine relevant ranges of PWR end-of-life (EOL) rod-internal pressure (RIP) values, as well as PCTs and rod-averaged gas temperatures. EPRI documented results for publicly available PWR EOL RIP data at 25°C [20]. Characterization of the sister rods will result in up to 25 valuable data points for EOL RIP for standard PWR fuel rods. In particular, the examination of M5®-clad fuel rods will represent a significant improvement in the database as the current database does not include such fuel rods. In addition, Oak Ridge National Laboratory (ORNL) used FRAPCON to predict gas pressures for over 68,000 fuel rods irradiated during Cycles 1–12 in the Watts Bar Nuclear Unit 1 reactor [21]. The calculations documented in Ref. 21 were consistent with the database documented in Ref. 20 for standard PWR fuel rods. Both the database and the calculations for standard PWR fuel rods irradiated to 40–60 GWd/MTU were bounded by 5 MPa EOL RIP at 25°C.

The NRC sponsored the Pacific Northwest National Laboratory (PNNL) to perform FRAPCON calculations under drying and storage conditions for boiling water reactor, standard PWR, and IFBA PWR fuel rods using a validated model for gas release from the B-10-containing neutron absorber on the outer surface of fuel pellets for IFBA fuel rods [22].

The database [20] and FRAPCON predictions [21,22] for standard PWR fuel rods are summarized in Fig. 35. For burnups in the range of 40–60 GWd/MTU and initial He-fill pressures of 2.00–3.45 MPa, the EOL

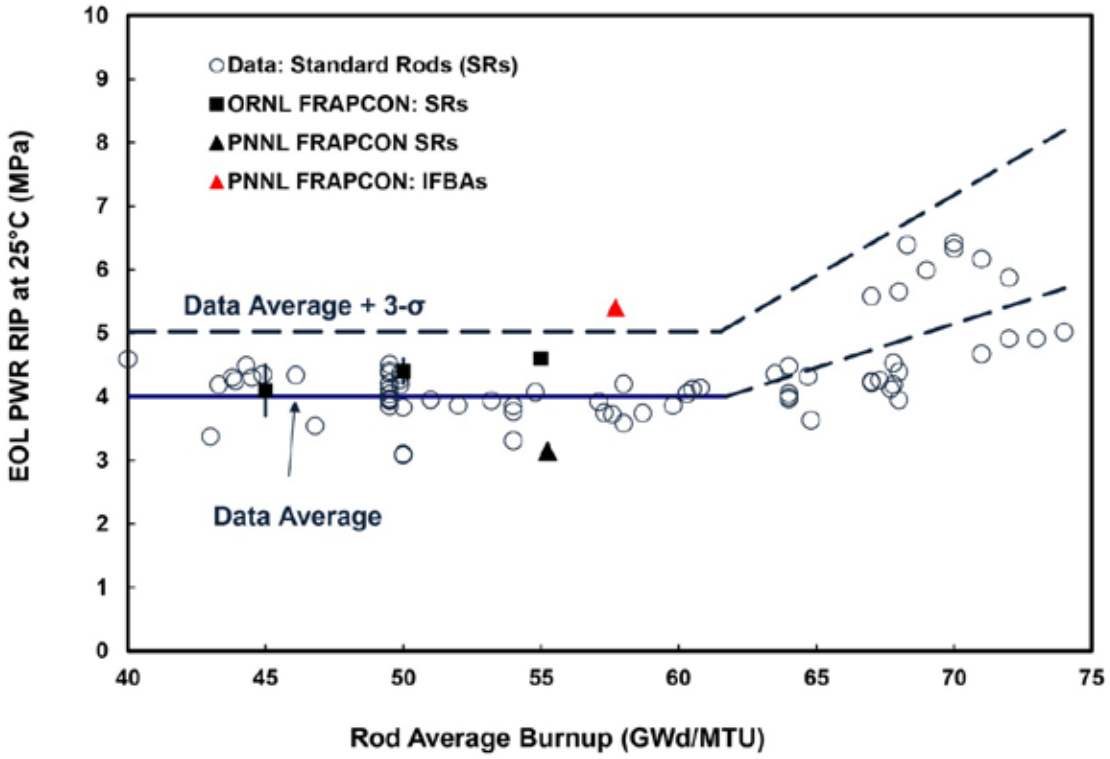

Figure 35: Measured and predicted EOL RIP values at 25°C.

RIP values are relatively flat with an average value of 4 MPa and a 3-sigma upper limit of 5 MPa. These results are significant because hoop stresses for fuel rods at PCT values relevant to drying, transfer, and storage would be too low to induce radial hydride embrittlement. ORNL has determined EOL RIP values for eight fuel rods in the burnup range of 49–59 GWd/MTU [23]. The EOL RIP values at 25°C are in the range of 3.2–4.7 MPa, which are below 5 MPa.

Sister Rod Post-Irradiation Examinations and Measured/Calculated Transportation Loads

The 25 sister rods include a wide range of linear heat ratings and cladding temperature gradients. In the Argonne study, a significant difference was observed between Zry-4 cladding from low-power fuel rods and ZIRLO™ cladding from high-power fuel rods. These differences may have had more to do with the differences in distribution of circumferential hydrides across the cladding wall than with the differences in alloys. Post-irradiation examinations (PIE) and testing of sister-rod cladding will resolve this issue. Reference 24 describes the PIE and testing planned for Phase 1 of the sister rod test program.

The SFWD-SFWST effort consists of three approaches for assessing cladding integrity during storage and post-storage transport: (a) ANL and PNNL will test defueled cladding RCT samples following RHT at 400°C and relevant internal pressures and corresponding cladding hoop stresses; (b) ORNL will perform similar RCTs using fueled cladding samples; and (c) Sandia National Laboratories (SNL) will continue to measure cladding strains during conditions of normal transport in conjunction with PNNL cask modeling efforts. It may be sufficient to demonstrate that defueled cladding retains ductility after RHT. As an added margin, ORNL results will likely show that the fuel limits cladding displacement, stresses, and strains due to pinch loading. Experimental and analytical results to date from the transportation effort

indicate that cladding strains are low and well within the elastic range for normal conditions of transport. These conditions also include a one-foot (0.3-m) drop, which has not yet been studied experimentally.

Data Trends

Data collected during the past five years suggest that radial-hydride-induced embrittlement may not occur in standard PWR fuel-rod cladding because EOL RIP values (<5 MPa at 25°C), PCTs (≤400°C), average gas temperatures (<400°C), and average assembly discharge burnups (<50 GWd/MTU) are all much lower than previously anticipated. Recent internal-pressure data from eight sister rods are consistent with available data for older PWR fuel rods (<5 MPa at 25°C). Best-estimate thermal models predict much lower PCT values for HBU PWR fuel rods during drying and storage. Low PCT values result in a significant reduction (e.g., from about 200 wppm at 400°C to about 80 wppm at 300°C) in the dissolved hydrogen available for radial-hydride precipitation. Low internal gas pressures (e.g., <10 MPa at 300°C) result in stresses too low to induce significant radial-hydride precipitation even if more hydrogen were available for precipitation. Additional internal-pressure data will be generated for ten fuel rods during Phase 1 of the sister-rod test program and up to seven data points will be generated during Phase 2. If the current trend of low rod-internal pressures continues, then cladding ductility decrease for standard PWR fuel rods would be due to high concentrations of circumferential hydrides found in Zircaloy-4, low-tin Zircaloy-4 and ZIRLO® fuel rods irradiated to HBU. The ductility of high-hydrogen-content cladding will also be determined in Phase 1 of the sister-rod test plan.

No EOL RIP values are available for IFBA rods. The PNNL FRAPCON predictions for peak cladding hoop stress for IFBA rods irradiated to about 58 GWd/MTU were <90 MPa (≤88.1 MPa) for 400°C PCT, plenum temperatures in the range of 264°C to 397°C, and internal cask pressures of 0.0004 MPa (near vacuum), 0.1 MPa (medium natural convection), and 0.69 MPa (high natural convection). The drying and storage temperatures represent upper-bound values, but the predicted EOL RIP extrapolated to 25°C may not represent an upper bound for IFBA rods. Assuming a 10% uncertainty in these FRAPCON calculations, the upper bound for peak cladding hoop stress would be 97 MPa, which is slightly higher than the transition hoop stress for ZIRLO® (90±3 MPa) suggested by the Argonne data. The FRAPCON calculations will be repeated after Phase 1 sister-rod data become available for EOL RIP and EOL free volume and these data are used to fine-tune fuel models in FRAPCON.

REFERENCES

[1] Geelhood, K.J., W.G. Lusher, and C.E. Beyer, *PNNL Stress/Strain Correlation for Zircaloy*, Pacific Northwest National Laboratory Report PNNL-17700, July 2008.

[2] Geelhood, K.J., W.G. Lusher, and P.A. Raynaud, *Material Property Correlations: Comparison Between FRACAON-3.5, FRAPCON-1.5, and MATPRO*, NUREG/CR-7024, Rev. 1, October 31, 2014, ML14296A063.

[3] Nuclear Regulatory Commission, Interim Staff Guidance (ISG)-11, Revision 3, "Cladding Considerations for the Transportation and Storage of Spent Fuel," November 2003. ML033230335.

[4] Ahn, T., H. Akhavannik, G. Bjorkman, F.C. Chang, W. Reed, A., Rigato, D. Tang, R.D. Torres, B.H. White, and V. Wilson, *Dry Storage and Transportation of High Burnup Spent Nuclear Fuel*, NUREG-2224, July 2018 draft report for public comment.

[5] Billone, M.C., T.A. Burtseva, and Y. Yan, *Ductile-to-Brittle Transition Temperature for High-Burnup Zircaloy-4 and ZIRLO™ Cladding Alloys Exposed to Simulated Drying-Storage Conditions*, Argonne National Laboratory Report ANL-13/13, NRC ADAMS ML12181A238, Sept. 2012.

[6] Billone, M.C., T.A. Burtseva, and R.E. Einziger, "Ductile-to-Brittle Transition Temperature for High-Burnup Cladding Alloys Exposed to Simulated Drying-Storage Conditions," J. Nucl. Mater. **433**, 431–448 (2013).

[7] Billone, M.C., T.A. Burtseva, J.P. Dobrzynski, D.P. McGann, K. Byrne, Z. Han, and Y.Y. Liu, *Phase I Ring Compression Testing of High-Burnup Cladding*, FCRD-USED-2012-000039, Dec. 31, 2011.

[8] Billone, M.C., T.A. Burtseva, and Y.Y. Liu, *Baseline Studies for Ring Compression Testing of High-Burnup Fuel Cladding*, Argonne National Laboratory Report ANL-12/58, FCRD-USED-2013-000040, Nov. 23, 2012.

[9] Billone, M.C., T.A. Burtseva, and Y.Y. Liu, "Effects of Drying and Storage on High-Burnup Cladding Ductility," Proc. IHLRWMC, Albuquerque, NM, April 28–May 2, 2013, Paper 6973, 1106–1113 (2013).

[10] Billone, M.C., T.A. Burtseva, and Y.Y. Liu, "Baseline Properties and DBTT of High-Burnup PWR Cladding Alloys," Proc. PATRAM 2013, San Francisco, CA, August 18–23, 2013.

[11] Billone, M.C., T.A. Burtseva, Z. Han, and Y.Y. Liu, *Embrittlement and DBTT of High-Burnup PWR Fuel Cladding Alloys*, Argonne National Laboratory Report ANL-13/16, FCRD-UFD-2013-000401, Sept. 30, 2013.

[12] Billone, M.C., T.A. Burtseva, Z. Han, and Y.Y. Liu, *Effects of Multiple Drying Cycles on High-Burnup PWR Cladding Alloys*, Argonne National Laboratory Report ANL-14/11, FCRD-UFD-2014-000052, Sept. 26, 2014.

[13] Billone, M.C., T.A. Burtseva, and M.A. Martin-Rengel, *Effects of Lower Drying-Storage Temperatures on the DBTT of High-Burnup PWR Cladding*, Argonne National Laboratory Report ANL-15/21, FCRD-UFD-2015-000008, Aug. 28, 2015.

[14] Billone, M.C. and T.A. Burtseva, *Effects of Lower Drying-Storage Temperatures on the Ductility of High-Burnup PWR Cladding*, Argonne National Laboratory Report ANL-16/16, FCRD-UFD-2016-000065, Aug. 30, 2016.

[15] Billone, M.C. and T.A. Burtseva, *Effects of Radial Hydrides on PWR Cladding Ductility*, Argonne National Laboratory Report ANL-17/14, SFWD-SFWST-2017-000001, Sep. 13, 2017.

[16] Kearns, J.J., "Terminal Solubility and Partitioning of Hydrogen in the Alpha Phase of Zirconium, Zircaloy-2 and Zircaloy-4," J. Nucl. Mater. **22**, 292–303, 1967.

[17] Kammenzind, B.F., D.G. Franklin, H.R. Peters, and W.J. Duffin, "Hydrogen Pickup and Redistribution in Alpha-Annealed Zircaloy-4," *Zirconium in the Nuclear Industry: 11th Intl. Symp.*, ASTM STP 1295, E.R. Bradley and G.P. Sabol, Eds., ASTM, pp. 338–370, 1996.

[18] McMinn, A., E.C. Darby, and J.S. Schofield, "The Terminal Solid Solubility of Hydrogen in Zirconium Alloys, *Zirconium in the Nuclear Industry: 12th Intl. Symp.*, ASTM STP 1354, G.P. Sabol and G.D. Moan, Eds., ASTM, pp. 173–195, 2000.

[19] Tang, R. and X. Yang, "Dissolution and precipitation behaviors of hydrides in N18, Zry-4 and M5® alloys," Intl. J. Hydrogen Energy, **34** (2009) 7269–7274.

[20] Machiels, A., *End-of-Life Rod Internal Pressures in Spent Pressurized Water Reactor Fuel*, EPRI Report 3002001949, Dec. 2013.

[21] Bratton, R.N., M.A. Jessee, and W.A. Wieselquist, *Rod Internal Pressure Quantification and Distribution Analysis Using FRAPCON*, DOE Report FCRD-UFD-2015-000636, ORNL Report ORNL/TM-2015/557, Sept. 30, 2015.

[22] Richmond, D.J. and K.J. Geelhood, FRACON Analysis of Cladding Performance during Dry Storage Operations, PNNL-27418, April 2018.

[23] Bevard, Bruce, Rose Montgomery, Robert N. Morris, and John Scaglione, "Post-Irradiation Examinations of High-Burnup PWR Fuel Rods – Initial Results", TopFuel Conference, Prague, Czech Republic, October 2018.

[24] Saltzstein, Sylvia J., Mike Billone, Brady Hanson, and John Scaglione, "Visualization of the High-Burnup Spent Fuel Rod Phase 1 Test Plan: Technical Memo," SAND2018-8042 O, Jul. 18, 2018.